Table 2. Summary of statistical results for biomarkers

	Aβ1-42[a]	Aβ1-42/Aβ1-40[b]	APP669-711/Aβ1-42	PiB-mcSUVR
ANCOVA group comparisons				
PiB− (n = 22) mean (95% CI)	0.21 (0.18–0.24)	0.011 (0.009–0.012)	0.72 (0.63–0.82)	1.10 (0.98–1.21)
PiB+ (n = 40) mean (95% CI)	0.14 (0.12–0.15)	0.007 (0.006–0.008)	1.13 (1.07–1.19)	1.65 (1.57–1.72)
F-value	8.19	7.89	24.98	31.62
P-value	<0.001	0.001	<0.001	<0.001
coefficient of determination (η^2)	0.298	0.290	0.564	0.621
ROC analysis (PiB− vs PiB+, n = 62)				
area under the curve (AUC)	0.808	0.798	0.969	0.975
sensitivity	0.825	0.750	0.925	0.925
specificity	0.773	0.773	0.955	1.000
Multiple regression analysis (n = 62)				
model *R*	0.424	0.317	0.687	
F-value	6.48	3.30	26.44	
P-value	0.003	0.044	<0.001	
significance (*P*-value), mcSUVR/age	<0.001/0.094	0.016/0.841	<0.001/0.826	
single correlation (*r*), mcSUVR/age	−0.374/−0.060	−0.316/−0.085	0.687/0.217	
partial correlation (*r*), mcSUVR/age	−0.421/0.216	−0.307/0.026	0.668/−0.029	

Upper part: Results of analysis of covariance (ANCOVAs) for comparison between PiB− and PiB+ groups in biomarkers and PiB-mcSUVR. Values in parentheses represent 95% confidence interval (CI). All results are adjusted for age.
Middle part: Results of the receiver operating characteristic (ROC) analysis of biomarkers and PiB-mcSUVR to discriminate visually classified PiB− and PiB+ individuals (Fig. 3). The sensitivity indicates the true positive rate as calculated by (true positive)/((true positive) + (false negative)), and the specificity indicates the true negative rate as calculated by (true negative)/((false positive) + (true negative)). The AUC (the area under the ROC curve) express a kind of overall diagnostic accuracy. The cutoff values for Aβ1-42, Aβ1-42/Aβ1-40, APP669-711/Aβ1-42, and PiB-mcSUVR are 0.183, 0.009, 0.914, and 1.271, respectively.
Lower part: Results of the multiple regression analysis of biomarkers using PiB-mcSUVR and age as predictors. Also, results of the simple analysis of correlation (single correlation) to both PiB-mcSUVR and age, and results of partial correlation analysis adjusted for age or PiB-mcSUVR are shown.
[a]The values represent by the intensity of Aβ1-42 peak relative to that of SIL-Aβ1-38 peak as an internal standard.
[b]Note that the Aβ1-42/Aβ1-40 are markedly different from the reported values in other studies, because of methodological differences (see Results, Measurements of Aβs and AβAPs).

Performances of the plasma biomarkers. Since not Aβ1-42/APP669-711 but APP669-711/Aβ1-42 was normally distributed, the latter values were used for the statistical analyses. Therefore performances of the APP669-711/Aβ1-42 were compared with those of Aβ1-42 level and Aβ1-42/Aβ1-40. PiB-mcSUVR values were also analyzed as the ideal reference. All of the statistical results are summarized in Table 2.

Group comparisons between PiB− and PiB+ individuals. The upper part of Table 2 demonstrates the results of ANCOVA adjusted for age. Using our newly established method, the Aβ1-42 level showed a highly significant difference between the groups. Aβ1-42/Aβ1-40 did not improve the significant level; however, APP669-711/Aβ1-42 markedly enhanced the group-separation capability. The *F*-value and the effect size (η^2) of APP669-711/Aβ1-42 were comparable to those of PiB-mcSUVR.

Capability to discriminate PiB+ individuals from PiB− individuals. To evaluate the capability of APP669-711/Aβ1-42 to discriminate PiB+ individuals from PiB− ones, ROC analysis was performed. The results are shown in the middle part of Table 2 and Fig. 3. APP669-711/Aβ1-42 demonstrated an extremely high AUC (0.969). The sensitivity and specificity for the discriminative capability of APP669-711/Aβ1-42 were 0.925 (3 out of 40 were false negative) and 0.955 (1 out of 22 was false positive), respectively, with a cutoff value of 0.914. The performance indices of APP669-711/Aβ1-42 were also comparable to those of PiB-mcSUVR.

Correlation between our plasma biomarkers and PiB-mcSUVR. To evaluate the strength of the link between our plasma biomarkers and PiB-mcSUVR, we performed correlation and regression analyses. The results are shown in the lower part of Table 2 and Figs. 4A and 4B. All of the plasma biomarkers

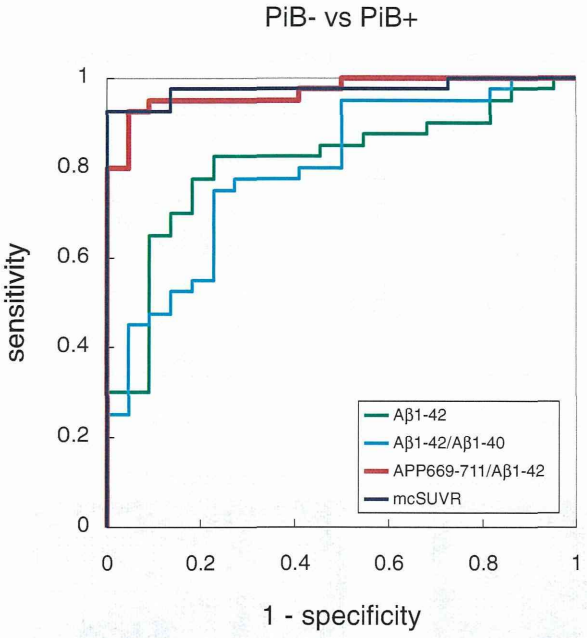

Fig. 3. ROC analysis of the biomarkers as discriminators of PiB+ and PiB− individuals. ROC curves of plasma biomarkers and PiB-mcSUVR are shown in discriminating PiB+ individuals from PiB− individuals. The associated statistical values are displayed in the middle part of Table 2.

showed statistically significant correlation with PiB-mcSUVR. In particular, APP669-711/Aβ1-42 demonstrated high correlation coefficients both in the simple correlation (single $r = 0.687$, $P < 0.001$) and the correlation adjusted for age (partial $r = 0.668$, $P < 0.001$) (Fig. 4A). Multiple regression analysis showed there were no significant ageing effects. Moreover, the regression analysis of PiB-SUVR images using biomarker levels as covariate vectors demonstrated that plasma APP669-711/Aβ1-42 significantly correlated with regional PiB retention (FWE corrected $P < 0.05$, $T = 5.18$, extent threshold $k = 200$ voxels). The visualized areas, robustly involving the frontal, precuneus, and posterior cingulate, and the parietotemporal cortices, appeared to correspond to the typical pattern of Aβ accumulation in AD (Fig. 4B, right).[29),30)] Although no significant clusters were found with the same threshold as the APP669-711/Aβ1-42 threshold, the results with a lowered threshold (uncorrected $P < 0.0001$, $T = 3.97$) suggest that the plasma Aβ1-42 level and Aβ1-42/Aβ1-40 also reflect the cortical Aβ accumulation (Fig. 4B, left and middle).

Performances across clinical categories. Additionally, the performances of the biomarkers were tested across the clinical categories. The results of ANCOVA (adjusted for age) demonstrate that APP669-711/Aβ1-42 showed highly significant group differences with a large effect size (Table 3, upper part), which were almost comparable to those of PiB-mcSUVR. The post-hoc group comparisons demonstrated that APP669-711/Aβ1-42 is sensitive in distinguishing between HC− and any other PiB+ groups (HC+, MCI and AD) (Fig. 5). On the other hand, APP669-711/Aβ1-42 appeared not so sensitive in distinguishing groups classified according to the clinical severity of AD. Within the PiB+ group, only a comparison between HC+ and AD showed a significant difference. We also conducted ROC analysis to evaluate the discriminative capability of the plasma biomarkers across the clinical categories (Table 3, lower part, and Fig. 6). APP669-711/Aβ1-42 showed very high sensitivity and specificity in discriminating HC-individuals from AD and MCI individuals. Importantly, the results demonstrated that APP669-711/Aβ1-42 could identify PiB+ individuals within a cognitively healthy group (HC− vs HC+) with 90.9% sensitivity and 90.9% specificity with a cut off value of 0.863.

Discussion

This study shows that APP669-711/Aβ1-42 in plasma has a big potential as a biomarker precisely surrogating cerebral amyloid deposition. Our biomarker clearly discriminated between PiB− and PiB+ groups with a large effect size ($\eta^2 = 0.56$), and the sensitivity and specificity in discriminating PiB+ individuals from PiB− individuals were very high (0.925 and 0.955, respectively). Furthermore, APP669-711/Aβ1-42 significantly correlated with cortical PiB retention with a high correlation coefficient (age-adjusted partial $r = 0.668$). As a surrogate marker for cerebral amyloid deposition, the performances of APP669-711/Aβ1-42 were far beyond those of reported plasma biomarkers[13),31),32)] and were comparable to those of CSF biomarkers.[27),28),33)] Considering invasiveness and cost, the clinical, as well as social, impact of our novel plasma biomarker would be very significant.

A great deal of effort has been made to determine whether plasma Aβs can be diagnostic and/or predictive biomarkers for AD; however, so far the results were contradictory and, in most studies, there was a broad overlap in the levels of plasma Aβs between controls and patients. This may be due to the difficulties in Aβ measurement in plasma, which are likely caused by various factors,[14)] including low

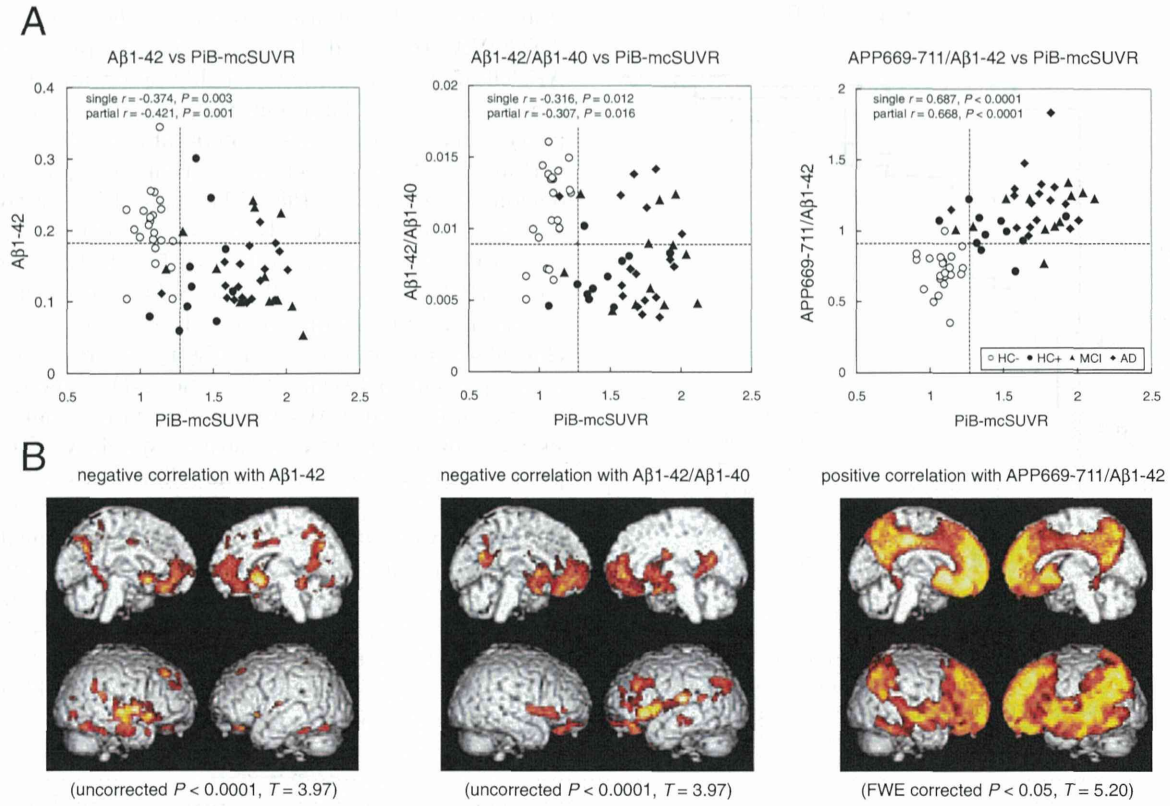

Fig. 4. Correlations between plasma biomarkers and PiB-mcSUVR. A) Scatter plots for biomarkers and PiB-mcSUVR. The open and closed symbols in the scatter plots indicate PiB− and PiB+ groups, respectively. The dashed lines represent cut-off values estimated by the ROC analyses as shown in Fig. 3 and Table 2. B) Regression analysis of PiB-SUVR images for each biomarker adjusted for age. Brain areas that showed statistically significant correlation between regional PiB retention and each biomarker are visualized. Please note that the height threshold of APP669-711/Aβ1-42 is different from the others. The extent thresholds of all are the same ($k = 200$ voxels).

Aβ concentrations and unavoidable Aβ binding to other proteins, which may mask the antibody epitope of Aβ.[34] The utility of the plasma Aβs as AD biomarkers may also be complicated by the fact that plasma Aβs can originate from peripheral organs.[2),35] In addition to these technical and biological aspects of plasma Aβs, the development of biomarkers for AD is generally hampered by a difficulty in correctly recruiting "control subjects" because a large proportion of cognitively normal aged individuals exhibit AD pathologic features, including cerebral amyloid deposition,[19)–21] which has recently been corroborated by amyloid PET studies.[36),37]

To overcome these obstacles, we designed this study as follows. First, to increase detection sensitivity and specificity, we employed our novel IP-MS system.[16] In this system, we used hetero-F(ab′) fragments of two monoclonal antibodies (6E10 and 4G8), which are specific to different Aβ epitopes, that were coupled to PEG on magnetic beads [hetero-F(ab′)-$(PEG)_{24}$ beads],[16] and then, the molecular species of the captured Aβs and AβAPs were precisely and simultaneously determined by MALDI-TOF MS. Compared with the performance of conventional sandwich ELISA measurements, the efficiency and accuracy of Aβ detection in our IP-MS system were markedly high.[17] Indeed, the performances of Aβ1-42 in the present study (Table 2, Figs. 3 and 4) were much higher than those in previous studies.[13),31),32] Second, to decipher the pathological significance of unpredictable changes of Aβ1-42 in plasma, we used APP669-711 as a reference against Aβ1-42. Using the APP669-711 to Aβ1-42 ratio, the performances were extremely high compared with those obtained from Aβ1-42 and Aβ1-40 (Table 2, Figs. 3 and 4). Third, to correctly classify participants in terms of cerebral amyloid deposition, we carried out PiB amyloid imaging by PET of all the subjects. By objective

Table 3. Summary of statistical results for biomarkers for discriminating across clinical categories

	Aβ1-42	Aβ1-42/Aβ1-40	APP669-711/Aβ1-42	PiB-mcSUVR
ANCOVA group comparisons				
HC− (n = 22) mean (95% CI)	0.21 (0.18–0.24)	0.011 (0.009–0.012)	0.72 (0.64–0.81)	1.10 (0.99–1.20)
HC+ (n = 11) mean (95% CI)	0.14 (0.11–0.17)	0.007 (0.005–0.009)	0.99 (0.88–1.09)	1.45 (1.33–1.57)
MCI (n = 12) mean (95% CI)	0.14 (0.10–0.17)	0.008 (0.006–0.010)	1.11 (1.01–1.21)	1.74 (1.61–1.86)
AD (n = 17) mean (95% CI)	0.14 (0.11–0.17)	0.008 (0.006–0.009)	1.24 (1.15–1.33)	1.74 (1.63–1.84)
F-value	5.21	3.52	15.22	19.23
P-value	<0.001	0.003	<0.001	<0.001
coefficient of determination (η^2)	0.403	0.313	0.664	0.714
ROC analysis				
HC− vs HC+ (AUC/sensitivity/specificity)	0.789/0.818/0.818	0.876/0.909/0.773	0.930/0.909/0.909	0.934/0.909/1.000
HC− vs MCI	0.746/0.667/0.909	0.803/0.750/0.773	0.966/0.917/1.000	0.989/0.917/1.000
HC− vs AD	0.864/0.941/0.773	0.743/0.706/0.727	0.997/1.000/0.955	0.992/0.941/1.000

Upper part: Results of the ANCOVA for comparisons among classified groups for biomarkers and PiB-mcSUVR. Values in the parentheses represent 95% confidence interval (CI). All results are adjusted for age. The post-hoc results are displayed in Fig. 5.
Lower part: Results of the receiver operating characteristics (ROC) analyses for each biomarker and PiB-mcSUVR to discriminate across the clinical categories; HC− vs. HC+, MCI, and AD. The cutoff value for each analysis was determined by the nearest point in the curve from the left upper corner. ROC curves are shown in Fig. 6.

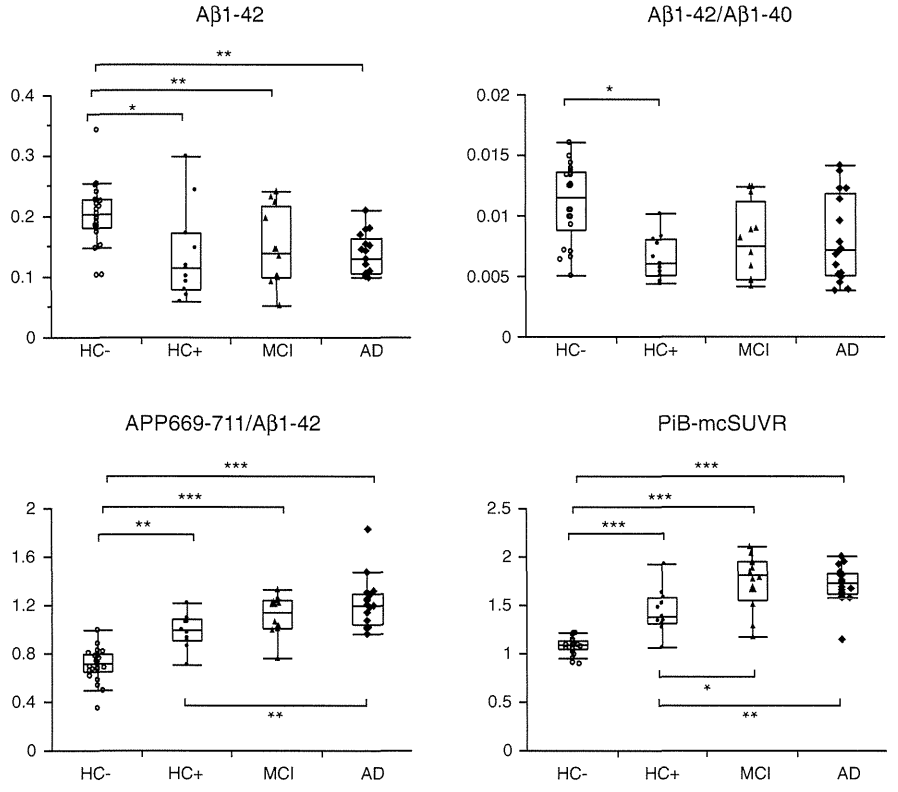

Fig. 5. Group comparisons of the plasma biomarkers and PiB-mcSUVR across clinical categories. Distribution of each value is shown by a box-whisker plot. The boxes represent the 25th, 50th (median) and 75th percentiles of the data. The ends of whiskers represent the lowest (or highest) datum within 1.5-times interquartile range from the 25th (or 75th) percentile. The plotted values were original, but the results of the multiple comparisons were adjusted for age. All p-values were Bonferroni corrected, and the significance levels are represented by the number of asterisks: $^*P < 0.05$, $^{**}P < 0.01$, $^{***}P < 0.001$.

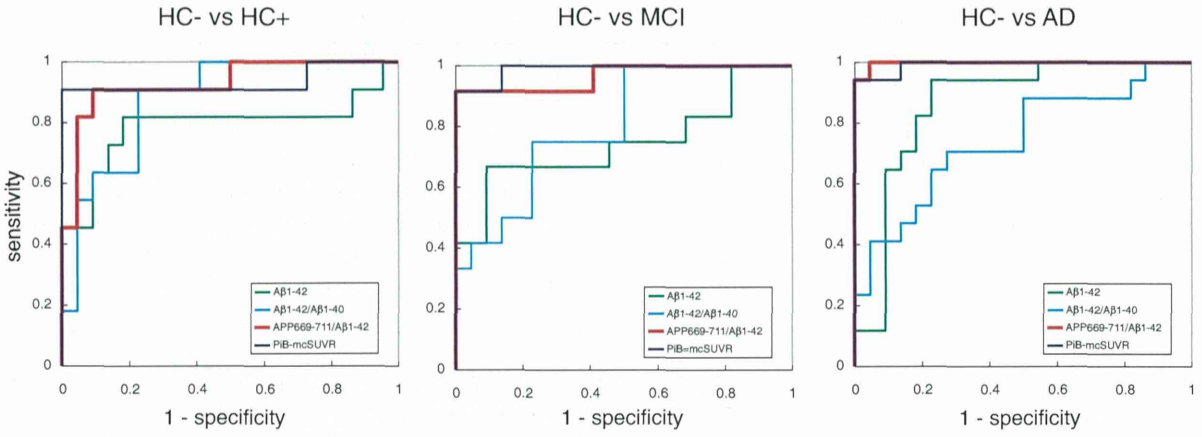

Fig. 6. ROC curves to discriminate across the clinical categories. ROC curves of the plasma biomarkers and PiB-mcSUVR to discriminate between HC− vs. HC+ (left), HC− vs. MCI (middle), and HC− vs. AD (right). The associated statistical values are displayed in the lower part of Table 3.

determination of the state of cerebral amyloid deposition in each participant, we were able to confirm the usefulness of our biomarkers.

It remains to be elucidated why the APP669-711/Aβ1-42 ratio in the plasma showed the highest significance in correlation with the presence of cerebral amyloid deposition. One possible explanation is as follows. APP669-711 has almost the same size and amino acid sequence as Aβ1-42; thus, these two peptides may show the same metabolism rate, binding tendency to other molecules in the brain and plasma, and also penetration capability through the blood-brain barrier. In contrast, the aggregation tendency of APP669-711 may be extremely lower than that of Aβ1-42 because of the difference in both amino- and carboxyl-termini. Collectively, the coexistence of similar and dissimilar characteristics of Aβ1-42 likely allows APP699-711 in plasma to function as a good reference against Aβ1-42.

In conclusion, we found that APP669-711/Aβ1-42 is a highly sensitive plasma biomarker that precisely surrogates cerebral amyloid deposition. This simple and minimally invasive biomarker should be beneficial in the clinical diagnoses of AD, possibly substituting the CSF examination. In addition, our biomarker can be a very powerful screening tool to identify people at risk of AD development from a community, and thereby likely facilitates development of disease-modifying clinical trials for AD.

Acknowledgments

We sincerely thank Drs. Hattori, Fukuda, Kawai, Horibe, and Konagaya for clinical evaluation of outpatients, and the staff of NCGG, particularly Ms. Honda as CRC, for recruiting participants, and collecting clinical data. This study was funded by a grant from the Japan Society for the Promotion of Science (JSPS) through the "Funding Program for World-Leading Innovative R&D of Science and Technology (FIRST)".

References

1) Blennow, K., Zetterberg, H. and Fagan, A.M. (2012) Fluid biomarkers in Alzheimer disease. Cold Spring Harb. Perspect. Med. **2**, a006221.
2) Henriksen, K., O'Bryant, S.E., Hampel, H., Trojanowski, J.Q., Montine, T.J., Jeromin, A., Blennow, K., Lönneborg, A., Wyss-Coray, T., Soares, H., Bazenet, C., Sjögren, M., Hu, W., Lovestone, S., Karsdal, M.A., Weiner, M.W. and Group, B.-B. B. I. (2014) The future of blood-based biomarkers for Alzheimer's disease. Alzheimers Dement. **10**, 115–131.
3) Fagan, A.M., Mintun, M.A., Mach, R.H., Lee, S.Y., Dence, C.S., Shah, A.R., LaRossa, G.N., Spinner, M.L., Klunk, W.E., Mathis, C.A., DeKosky, S.T., Morris, J.C. and Holtzman, D.M. (2006) Inverse relation between in vivo amyloid imaging load and cerebrospinal fluid Abeta42 in humans. Ann. Neurol. **59**, 512–519.
4) Pike, K.E., Savage, G., Villemagne, V.L., Ng, S., Moss, S.A., Maruff, P., Mathis, C.A., Klunk, W.E., Masters, C.L. and Rowe, C.C. (2007) Beta-amyloid imaging and memory in non-demented individuals: evidence for preclinical Alzheimer's disease. Brain **130**, 2837–2844.
5) Fagan, A.M., Head, D., Shah, A.R., Marcus, D., Mintun, M., Morris, J.C. and Holtzman, D.M. (2009) Decreased cerebrospinal fluid Abeta(42) correlates with brain atrophy in cognitively normal

elderly. Ann. Neurol. **65**, 176–183.
6) Jack, C.R., Knopman, D.S., Jagust, W.J., Shaw, L.M., Aisen, P.S., Weiner, M.W., Petersen, R.C. and Trojanowski, J.Q. (2010) Hypothetical model of dynamic biomarkers of the Alzheimer's pathological cascade. Lancet Neurol. **9**, 119–128.
7) Bateman, R.J., Xiong, C., Benzinger, T.L., Fagan, A.M., Goate, A., Fox, N.C., Marcus, D.S., Cairns, N.J., Xie, X., Blazey, T.M., Holtzman, D.M., Santacruz, A., Buckles, V., Oliver, A., Moulder, K., Aisen, P.S., Ghetti, B., Klunk, W.E., McDade, E., Martins, R.N., Masters, C.L., Mayeux, R., Ringman, J.M., Rossor, M.N., Schofield, P.R., Sperling, R.A., Salloway, S., Morris, J.C. and Network, D.I.A. (2012) Clinical and biomarker changes in dominantly inherited Alzheimer's disease. N. Engl. J. Med. **367**, 795–804.
8) Villemagne, V.L., Burnham, S., Bourgeat, P., Brown, B., Ellis, K.A., Salvado, O., Szoeke, C., Macaulay, S.L., Martins, R., Maruff, P., Ames, D., Rowe, C.C. Masters, C.L. and Group, A. I. B. a. L. A. R. (2013) Amyloid β deposition, neurodegeneration, and cognitive decline in sporadic Alzheimer's disease: a prospective cohort study. Lancet Neurol. **12**, 357–367.
9) Jack, C.R., Knopman, D.S., Jagust, W.J., Petersen, R.C., Weiner, M.W., Aisen, P.S., Shaw, L.M., Vemuri, P., Wiste, H.J., Weigand, S.D., Lesnick, T.G., Pankratz, V.S., Donohue, M.C. and Trojanowski, J.Q. (2013) Tracking pathophysiological processes in Alzheimer's disease: an updated hypothetical model of dynamic biomarkers. Lancet Neurol. **12**, 207–216.
10) Rissman, R.A., Trojanowski, J.Q., Shaw, L.M. and Aisen, P.S. (2012) Longitudinal plasma amyloid beta as a biomarker of Alzheimer's disease. J. Neural Transm. **119**, 843–850.
11) Rembach, A., Faux, N.G., Watt, A.D., Pertile, K.K., Rumble, R.L., Trounson, B.O., Fowler, C.J., Roberts, B.R., Perez, K.A., Li, Q.X., Laws, S.M., Taddei, K., Rainey-Smith, S., Robertson, J.S., Vandijck, M., Vanderstichele, H., Barnham, K.J., Ellis, K.A., Szoeke, C., Macaulay, L., Rowe, C.C., Villemagne, V.L., Ames, D., Martins, R.N., Bush, A.I., Masters, C.L. and group, A. r. (2014) Changes in plasma amyloid beta in a longitudinal study of aging and Alzheimer's disease. Alzheimers Dement. **10**, 53–61.
12) Figurski, M.J., Waligórska, T., Toledo, J., Vanderstichele, H., Korecka, M., Lee, V.M., Trojanowski, J.Q., Shaw, L.M. and Initiative, A. s. D. N. (2012) Improved protocol for measurement of plasma β-amyloid in longitudinal evaluation of Alzheimer's Disease Neuroimaging Initiative study patients. Alzheimers Dement. **8**, 250–260.
13) Song, F., Poljak, A., Valenzuela, M., Mayeux, R., Smythe, G.A. and Sachdev, P.S. (2011) Meta-analysis of plasma amyloid-β levels in Alzheimer's disease. J. Alzheimers Dis. **26**, 365–375.
14) Toledo, J.B., Vanderstichele, H., Figurski, M., Aisen, P.S., Petersen, R.C., Weiner, M.W., Jack, C.R., Jagust, W., Decarli, C., Toga, A.W., Toledo, E., Xie, S.X., Lee, V.M., Trojanowski, J.Q., Shaw, L.M. and Initiative, A. s. D. N. (2011) Factors affecting Aβ plasma levels and their utility as biomarkers in ADNI. Acta Neuropathol. **122**, 401–413.
15) Toledo, J.B., Shaw, L.M. and Trojanowski, J.Q. (2013) Plasma amyloid beta measurements—a desired but elusive Alzheimer's disease biomarker. Alzheimers Res. Ther. **5**, 8.
16) Kaneko, N., Yoshimori, T., Yamamoto, R., Capon, D.J., Shimada, T., Sato, T.A. and Tanaka, K. (2013) Multi epitope-targeting immunoprecipitation using F(ab′) fragments with high affinity and specificity for the enhanced detection of a peptide with matrix-assisted laser desorption ionization-time-of-flight mass spectrometry. Anal. Chem. **85**, 3152–3159.
17) Kaneko, N., Yamamoto, R., Sato, T.A. and Tanaka, K. (2014) Identification and quantification of amyloid beta-related peptides in human plasma using matrix-assisted laser desorption/ionization time-of-flight mass spectrometry. Proc. Jpn. Acad., Ser. B, Phys. Biol. Sci. **90**, 104–117.
18) De Meyer, G., Shapiro, F., Vanderstichele, H., Vanmechelen, E., Engelborghs, S., De Deyn, P.P., Coart, E., Hansson, O., Minthon, L., Zetterberg, H., Blennow, K., Shaw, L., Trojanowski, J.Q. and Initiative, A. s. D. N. (2010) Diagnosis-independent Alzheimer disease biomarker signature in cognitively normal elderly people. Arch. Neurol. **67**, 949–956.
19) Snowdon, D.A. (1997) Aging and Alzheimer's disease: lessons from the Nun Study. Gerontologist **37**, 150–156.
20) Price, J.L. and Morris, J.C. (1999) Tangles and plaques in nondemented aging and "preclinical" Alzheimer's disease. Ann. Neurol. **45**, 358–368.
21) Davis, D.G., Schmitt, F.A., Wekstein, D.R. and Markesbery, W.R. (1999) Alzheimer neuropathologic alterations in aged cognitively normal subjects. J. Neuropathol. Exp. Neurol. **58**, 376–388.
22) McKhann, G.M., Knopman, D.S., Chertkow, H., Hyman, B.T., Jack, C.R., Kawas, C.H., Klunk, W.E., Koroshetz, W.J., Manly, J.J., Mayeux, R., Mohs, R.C., Morris, J.C., Rossor, M.N., Scheltens, P., Carrillo, M.C., Thies, B., Weintraub, S. and Phelps, C.H. (2011) The diagnosis of dementia due to Alzheimer's disease: recommendations from the National Institute on Aging-Alzheimer's Association workgroups on diagnostic guidelines for Alzheimer's disease. Alzheimers Dement. **7**, 263–269.
23) Albert, M.S., DeKosky, S.T., Dickson, D., Dubois, B., Feldman, H.H., Fox, N.C., Gamst, A., Holtzman, D.M., Jagust, W.J., Petersen, R.C., Snyder, P.J., Carrillo, M.C., Thies, B. and Phelps, C.H. (2011) The diagnosis of mild cognitive impairment due to Alzheimer's disease: recommendations from the National Institute on Aging-Alzheimer's Association workgroups on diagnostic guidelines for Alzheimer's disease. Alzheimers

Dement. **7**, 270–279.
24) Rabinovici, G.D., Rosen, H.J., Alkalay, A., Kornak, J., Furst, A.J., Agarwal, N., Mormino, E.C., O'Neil, J.P., Janabi, M., Karydas, A., Growdon, M.E., Jang, J.Y., Huang, E.J., Dearmond, S.J., Trojanowski, J.Q., Grinberg, L.T., Gorno-Tempini, M.L., Seeley, W.W., Miller, B.L. and Jagust, W.J. (2011) Amyloid vs FDG-PET in the differential diagnosis of AD and FTLD. Neurology **77**, 2034–2042.
25) Tzourio-Mazoyer, N., Landeau, B., Papathanassiou, D., Crivello, F., Etard, O., Delcroix, N., Mazoyer, B. and Joliot, M. (2002) Automated anatomical labeling of activations in SPM using a macroscopic anatomical parcellation of the MNI MRI single-subject brain. Neuroimage **15**, 273–289.
26) Vandenberghe, R., Van Laere, K., Ivanoiu, A., Salmon, E., Bastin, C., Triau, E., Hasselbalch, S., Law, I., Andersen, A., Korner, A., Minthon, L., Garraux, G., Nelissen, N., Bormans, G., Buckley, C., Owenius, R., Thurfjell, L., Farrar, G. and Brooks, D.J. (2010) 18F-flutemetamol amyloid imaging in Alzheimer disease and mild cognitive impairment: a phase 2 trial. Ann. Neurol. **68**, 319–329.
27) Irwin, D.J., McMillan, C.T., Toledo, J.B., Arnold, S.E., Shaw, L.M., Wang, L.S., Van Deerlin, V., Lee, V.M., Trojanowski, J.Q. and Grossman, M. (2012) Comparison of cerebrospinal fluid levels of tau and Aβ 1-42 in Alzheimer disease and frontotemporal degeneration using 2 analytical platforms. Arch. Neurol. **69**, 1018–1025.
28) Jagust, W.J., Landau, S.M., Shaw, L.M., Trojanowski, J.Q., Koeppe, R.A., Reiman, E.M., Foster, N.L., Petersen, R.C., Weiner, M.W., Price, J.C., Mathis, C.A. and Initiative, A. s. D. N. (2009) Relationships between biomarkers in aging and dementia. Neurology **73**, 1193–1199.
29) Braak, H. and Braak, E. (1991) Neuropathological stageing of Alzheimer-related changes. Acta Neuropathol. **82**, 239–259.
30) Rowe, C.C., Ng, S., Ackermann, U., Gong, S.J., Pike, K., Savage, G., Cowie, T.F., Dickinson, K.L., Maruff, P., Darby, D., Smith, C., Woodward, M., Merory, J., Tochon-Danguy, H., O'Keefe, G., Klunk, W.E., Mathis, C.A., Price, J.C., Masters, C.L. and Villemagne, V.L. (2007) Imaging beta-amyloid burden in aging and dementia. Neurology **68**, 1718–1725.
31) Rembach, A., Watt, A.D., Wilson, W.J., Villemagne, V.L., Burnham, S.C., Ellis, K.A., Maruff, P., Ames, D., Rowe, C.C., Macaulay, S.L., Bush, A.I., Martins, R.N., Masters, C.L., Doecke, J.D. and Group, A.R. (2014) Plasma amyloid-β levels are significantly associated with a transition toward Alzheimer's disease as measured by cognitive decline and change in neocortical amyloid burden. J. Alzheimers Dis. **40**, 95–104.
32) Wang, T., Xiao, S., Liu, Y., Lin, Z., Su, N., Li, X., Li, G., Zhang, M. and Fang, Y. (2014) The efficacy of plasma biomarkers in early diagnosis of Alzheimer's disease. Int. J. Geriatr. Psychiatry **29**, 713–719.
33) Shaw, L.M., Vanderstichele, H., Knapik-Czajka, M., Clark, C.M., Aisen, P.S., Petersen, R.C., Blennow, K., Soares, H., Simon, A., Lewczuk, P., Dean, R., Siemers, E., Potter, W., Lee, V.M., Trojanowski, J.Q. and Initiative, A. s. D. N. (2009) Cerebrospinal fluid biomarker signature in Alzheimer's disease neuroimaging initiative subjects. Ann. Neurol. **65**, 403–413.
34) Kuo, Y.M., Emmerling, M.R., Lampert, H.C., Hempelman, S.R., Kokjohn, T.A., Woods, A.S., Cotter, R.J. and Roher, A.E. (1999) High levels of circulating Abeta42 are sequestered by plasma proteins in Alzheimer's disease. Biochem. Biophys. Res. Commun. **257**, 787–791.
35) Mehta, P.D., Pirttilä, T., Mehta, S.P., Sersen, E.A., Aisen, P.S. and Wisniewski, H.M. (2000) Plasma and cerebrospinal fluid levels of amyloid beta proteins 1–40 and 1–42 in Alzheimer disease. Arch. Neurol. **57**, 100–105.
36) Rowe, C.C., Ellis, K.A., Rimajova, M., Bourgeat, P., Pike, K.E., Jones, G., Fripp, J., Tochon-Danguy, H., Morandeau, L., O'Keefe, G., Price, R., Raniga, P., Robins, P., Acosta, O., Lenzo, N., Szoeke, C., Salvado, O., Head, R., Martins, R., Masters, C.L., Ames, D. and Villemagne, V.L. (2010) Amyloid imaging results from the Australian Imaging, Biomarkers and Lifestyle (AIBL) study of aging. Neurobiol. Aging **31**, 1275–1283.
37) Landau, S.M., Mintun, M.A., Joshi, A.D., Koeppe, R.A., Petersen, R.C., Aisen, P.S., Weiner, M.W., Jagust, W.J. and Initiative, A. s. D. N. (2012) Amyloid deposition, hypometabolism, and longitudinal cognitive decline. Ann. Neurol. **72**, 578–586.

(Received Sep. 5, 2014; accepted Sep. 25, 2014)

Ann Nucl Med
DOI 10.1007/s12149-015-0948-8

ORIGINAL ARTICLE

Radiosynthesis and in vivo evaluation of two imidazopyridineacetamides, [^{11}C]CB184 and [^{11}C]CB190, as a PET tracer for 18 kDa translocator protein: direct comparison with [^{11}C](*R*)-PK11195

Kentaro Hatano · Katsuhiko Sekimata · Takashi Yamada · Junichiro Abe · Kengo Ito · Mikako Ogawa · Yasuhiro Magata · Jun Toyohara · Kiichi Ishiwata · Giovanni Biggio · Mariangela Serra · Valentino Laquintana · Nunzio Denora · Andrea Latrofa · Giuseppe Trapani · Gaetano Liso · Hiromi Suzuki · Makoto Sawada · Masahiko Nomura · Hiroshi Toyama

Received: 27 June 2014 / Accepted: 14 January 2015

Abstract
Objective We report synthesis of two carbon-11 labeled imidazopyridines TSPO ligands, [^{11}C]CB184 and [^{11}C]CB190, for PET imaging of inflammatory process along with neurodegeneration, ischemia or brain tumor. Biodistribution of these compounds was compared with that of [^{11}C]CB148 and [^{11}C](*R*)-PK11195.
Methods Both [^{11}C]CB184 and [^{11}C]CB190 having ^{11}C-methoxyl group on an aromatic ring were readily prepared using [^{11}C]methyl triflate. Biodistribution and metabolism of the compounds were examined with normal mice. An animal PET study using 6-hydroxydopamine treated rats as a model of neurodegeneration was pursued for proper estimation of feasibility of the radioligands to determine neuroinflammation process.
Results [^{11}C]CB184 and [^{11}C]CB190 were obtained via *O*-methylation of corresponding desmethyl precursor using [^{11}C]methyl triflate in radiochemical yield of 73 % (decay-corrected). In vivo validation as a TSPO radioligand was carried out using normal mice and lesioned rats. In mice, [^{11}C]CB184 showed more uptake and specific binding than [^{11}C]CB190. Metabolism studies showed that 36 % and 25 % of radioactivity in plasma remained unchanged 30 min after intravenous injection of [^{11}C]CB184 and [^{11}C]CB190, respectively. In the PET study using rats, lesioned side of the brain showed significantly higher uptake than contralateral side after i.v. injection of either [^{11}C]CB184 or [^{11}C](*R*)-PK11195. Indirect Logan plot analysis revealed distribution volume ratio (DVR) between the two sides which might indicate lesion-related elevation of TSPO binding. The DVR was 1.15 ± 0.10 for [^{11}C](*R*)-PK11195 and was 1.15 ± 0.09 for [^{11}C]CB184.
Conclusion The sensitivity to detect neuroinflammation activity was similar for [^{11}C]CB184 and [^{11}C](*R*)-PK11195.

K. Hatano · K. Sekimata · T. Yamada · J. Abe · K. Ito
Department of Clinical and Experimental Neuroimaging, Center for Development of Advanced Medicine for Dementia, National Center for Geriatrics and Gerontology, Obu, Aichi 474-8522, Japan

Present Address:
K. Hatano (✉)
Faculty of Medicine, University of Tsukuba, Tsukuba 305-8575, Japan
e-mail: hatanok@md.tsukuba.ac.jp

M. Ogawa · Y. Magata
Medical Photonics Research Center, Hamamatsu University School of Medicine, Hamamatsu, Shizuoka 431-3192, Japan

J. Toyohara · K. Ishiwata
Research Team for Neuroimaging, Tokyo Metropolitan Institute of Gerontology, Tokyo 173-0015, Japan

G. Biggio · M. Serra
Department of Experimental Biology, University of Cagliari, 09100 Cagliari, Italy

V. Laquintana · N. Denora · A. Latrofa · G. Trapani · G. Liso
Pharmaco-Chemistry Department, University of Bari, Via Orabona 4, 70125 Bari, Italy

H. Suzuki · M. Sawada
Research Institute of Environmental Medicine, Nagoya University, Nagoya, Aichi 464-8601, Japan

M. Nomura · H. Toyama
Department of Radiology, Fujita Health University, Toyoake, Aichi 470-1192, Japan

Published online: 24 January 2015

Keywords Positron emission tomography · TSPO · PBR · Neuroinflammation · Alzheimer's disease

Introduction

Translocator protein (18 kDa) (TSPO) formerly referred to as peripheral benzodiazepine receptor (PBR) is a transmembrane multimeric protein complex primarily located in the outer mitochondrial membrane of cells [1]. It is especially concentrated in the outer/inner mitochondrial membrane contact sites [2], where it has been suggested to form a complex with other proteins such as the voltage-dependent anion channel and the adenine nucleotide transporter [3, 4]. TSPO is involved in various cell functions including porphyrin transport, heme biosynthesis, cholesterol transport, cell proliferation, apoptosis and anion transport [reviewed in 5, 6]. In central nervous system (CNS), TSPO is considered an ideal marker molecule for microglia activation [7]. Microglia undergo changes from a resting to an activated phenotype in response to a wide variety of CNS insults such as infectious diseases, inflammation, trauma, ischemia, brain tumors and neurodegeneration [8, 9]. Accumulation of a TSPO radioligand in lesioned area of brain is believed to be related with this microglia activation, and this is a key concept of clinical imaging of degenerative disorders of brain such as Alzheimer's disease by the means of positron emission tomography (PET) and this type of radioligand [7]. Our group reported that uptake of a TSPO radioligand, [^{11}C](*R*)-PK11195 was more related to this activation than number of the microglia cells [10] and suggested unknown mechanisms underlying the facilitated uptake of a TSPO radioligand.

[^{11}C](*R*)-PK11195 was the first TSPO radioligand applied to CNS diseases involving neuroinflammation process with PET [11]. Many clinical brain imaging studies were reported [reviewed in 8], however, the high degree of nonspecific uptake of [^{11}C](*R*)-PK11195 complicates the quantification and modeling of the PET data [12–15]. This significantly limits its sensitivity in detecting brain disorders. In this consequence, numerous radioligands for TSPO have been reported (Fig. 1). Zhang first reported carbon-11 labeled phenoxyphenyl acetamide, DAA1106 [16] and its fluoroalkyl congeners [17]. Briard reported structurally related phenoxypyridinyl acetamide, [^{11}C]PBR28 [18] and later Wilson also offered its fluoroalkyl congener, [^{18}F]FEPPA [19]. Another structural category should be referred to as "heterocyclic acetamide". Kassiou and coworkers reported pyrazolopyrimidinyl acetamides, [^{11}C]DPA-713 [20] and [^{18}F]DPA-714 [21]. Another example was dihydropurinylacetamide, [^{11}C]AC-5216 contributed by Zhang et al. [22]. Mattner offered I-123 labeled imidazopyridineacetamide, [^{123}I]CLINDE, for single photon emission computed tomography imaging [23].

We also reported four compounds of this class [24]. Only compound **[^{11}C]7** in the paper which is currently renamed as [^{11}C]CB148 showed satisfactory performance as a TSPO ligand in vivo. In the present article we report another two imidazopyridines, [^{11}C]CB184 and [^{11}C]CB190, with an ^{11}C-methoxyl group on an aromatic ring (Fig. 2). Feasibility of the compounds was examined

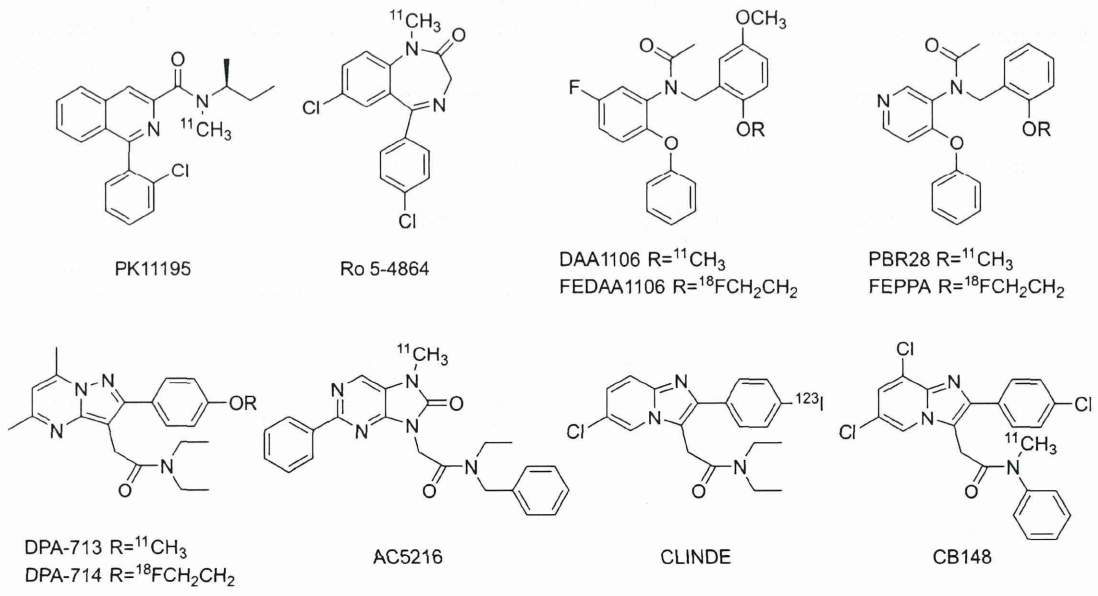

Fig. 1 Structures of TSPO radioligands

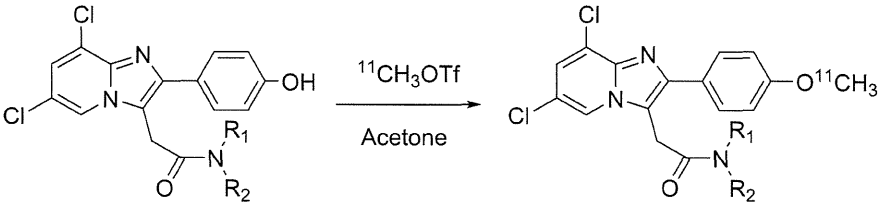

CB185 R_1=*n*-Pr, R_2=*n*-Pr
CB189 R_1=Me, R_2=*n*-Bu

CB184 R_1=*n*-Pr, R_2=*n*-Pr
CB190 R_1=Me, R_2=*n*-Bu

Fig. 2 Scheme of radiosynthesis

using intact mice following our previous report. In addition to this, we employed rat injury model of neurodegenerative disease. Measurement using high resolution animal PET and precise posthumous examination of the animals would reveal relevance of the methodology as well as the feasibility of the compounds in more persuasive manner, although there exist some difficulties pursuing this type of animal model study such as measurement and quantification method or appropriateness of the animal employed as human disease model. This study indicates proper direction for examining TSPO ligand performance.

Materials and methods

General

Reverse-phase high performance liquid chromatography (HPLC) was performed using LC-10A HPLC system (Shimadzu, Kyoto, Japan) accompanied by gamma ray detection using a NaI (Tl) scintillation system. An automated gamma counter with a NaI (Tl) detector (COBRA, Packard Instrument, Meriden, CT) was used to measure the radioactivity of samples from animal and partition coefficient studies. Male ddY mice and Wistar rats were supplied by Japan SLC (Hamamatsu, Japan) and Nihon Charles River (Tokyo, Japan), respectively. The present animal study was approved by the institutional committees for animal studies. Racemic PK11195 was purchased from Sigma (St. Louis, MO) and 0.1 M lithium aluminum hydride solution in tetrahydrofuran and a desmethyl derivative of (*R*)-PK11195 was purchased from ABX (Radeberg, Germany). Other chemicals were purchased from Kanto Chemicals (Tokyo, Japan) and were of the highest grade commercially available. All statistical analyses were carried out using StatView (SAS Institute Inc., Cary, NC).

Radiochemical syntheses

Unlabeled reference standard of CB184 and CB190 and their precursors, CB185 and CB189 were prepared according to previously reported method [25]. Carbon-11 was produced by $^{14}N(p, \alpha)^{11}C$ nuclear reaction using a CYPRIS HM18 cyclotron (Sumitomo Heavy Industries, Tokyo, Japan). $[^{11}C]CO_2$ thus obtained was converted to [^{11}C]methyl triflate using an automated synthesis system (CUPID C-11-BII, Sumitomo Heavy Industries, Tokyo, Japan). The obtained [^{11}C]methyl triflate was trapped in 0.3 mL acetone solution of containing 1 mg of CB185 or CB189 and 0.4 mg of NaOH (Fig. 3). The mixture was then heated at 80 °C for 3 min allowing the methylation reaction to occur. HPLC fractions containing purified [^{11}C]CB184 or [^{11}C]CB190 were collected into an evaporating vessel (HPLC conditions are summarized in Table 1). After removal of solvent, the residue was redissolved in the appropriate solvent and analyzed by reverse-phase HPLC (Table 1). The specific radioactivity of compounds was calculated by comparing the injected radioactivity with the corresponding UV peak area at 250 nm. Radiochemical synthesis of [^{11}C](*R*)-PK11195 was reported elsewhere [26].

Binding affinity and octanol/water partition coefficient

Binding affinity toward TSPO and central benzodiazepine receptor (CBR) and partition coefficient (Log *P*) were measured according to our previous report [24]. Separately, Log *P* value was calculated with CLOGP program [24].

Biodistribution in mice

A solution of [^{11}C]CB184, [^{11}C]CB190 or [^{11}C](*R*)-PK11195 in physiological saline containing 0.25 % polysorbate 80 (4 MBq/0.1 mL, 60–180 ng) was injected in male ddY mice (8–10 weeks old, 33–38 g, $n = 4$ for each group) via the tail vein. The mice were euthanized at 1, 15, 30 and 60 min after injection. Blood was removed by heart puncture using a syringe. Brain was dissected into olfactory bulb, cerebral cortex, striatum, thalamus, midbrain, cerebellum, and pons. The organs and the brain areas were weighed and the radioactivity was measured with a gamma counter. The raw counts were decay corrected to a standard

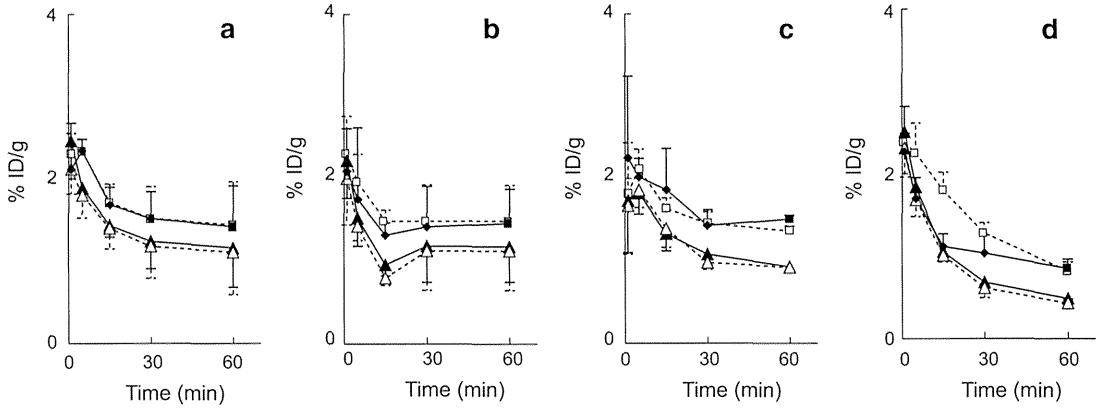

Fig. 3 Regional brain distribution; regional brain distribution of radioactivity after tail-vein injection of [^{11}C]CB184, [^{11}C]CB190, [^{11}C]CB148 and [^{11}C](*R*)-PK11195 in ddY mice is shown in **a–d**, respectively. Data are expressed as percentage of the injected dose per gram of tissue (%ID/g, mean and SD of four animals). *open circle* cerebellum, *filled circle* thalamus, *open triangle* cortex, *filled triangle* olfactory bulb. Data of [^{11}C]CB148 (**c**) was taken from literature [24]

Table 1 HPLC conditions

Compound	*Eluent*	*Flow rate (mL/min)*	*Retention time (min)*
Preparative			
CB184	Acetonitrile:H_2O (6:4)	6	9.1
CB190	Acetonitrile:H_2O (55:45)	6	10.1
Analytical			
CB185	Acetonitrile:H_2O (7:3)	1	7.8
CB190	Acetonitrile:H_2O (65:35)	1	8.0

Conditions employed for preparative and analytical HPLC are shown. Preparative HPLC was carried out using a Capcellpak C18 UG120S-5 μm column (10 mm inner diameter (i.d.) × 250 mm, Shiseido, Tokyo, Japan) and a JASCO HPLC system (JASCO, Tokyo, Japan) installed within the radiosynthesis system. Analytical HPLC was conducted using a Capcellpak C18 UG120S-5 μm column (4.8 mm i.d. × 250 mm, Shiseido, Tokyo, Japan) and a Shimadzu HPLC system (Shimadzu, Kyoto, Japan) with gamma ray detection using NaI(Tl) scintillator

time and the results were expressed as percentage of the injected does per gram of tissue (%ID/g).

Blocking studies

Mice (9–10 weeks old, 35–38 g, $n = 4$) were given via the tail vein with 0.1 mL of PK11195 in DMSO or flumazenil in physiological saline. All drugs were administered at dose of 1 mg/kg. A solution of each radioligand (prepared as above, 4 MBq/0.1 mL, 60–170 ng) was injected at 1 min after the cold drug treatment. At 30 min post-injection of the radioligand, the mice were euthanized and processed to measure %ID/g as above. Data were analyzed one-way ANOVA with Bonferroni's correction. Differences were considered significant at a p value less than 0.0167.

Metabolite studies

[^{11}C]CB184 or [^{11}C]CB190 (50–167 MBq, 0.46–1.1 μg) was intravenously injected into mice (8–9 weeks old, 36–39 g, $n = 3$ for each tracer), and 30 min later they were killed by cervical dislocation. Blood was removed by heart puncture using a heparinized syringe, and the brain was removed. After centrifugation of the blood at 7,000×g for 1 min at 4 °C the plasma of obtained, and 0.2–0.3 mL of the plasma was diluted with water up to 0.5 mL and denatured with 0.5 mL of acetonitrile in an ice-water bath. The suspension of plasma was centrifuged in the same condition and divided into soluble and precipitable fractions. The precipitate was re-suspended in 0.5 ml of acetonitrile followed by centrifugation. This procedure was repeated twice. The cerebellum (61–80 mg) was homogenized in 1 mL of a mixture of acetonitrile/water (1/1, v/v). The homogenate was treated as described above. Radioactivity in the three soluble fractions and precipitates was measured with gamma counter. In this treatment, the recovery yields in the soluble fraction were 80.3 ± 3.3 and 99.6 ± 0.1 % for plasma and brain, respectively, of mice given [^{11}C]CB184, and 96.6 ± 3.3 and 99.7 ± 0.3 % for plasma and brain, respectively, of mice given [^{11}C]CB190. The soluble fractions were combined and centrifuged as described above. A portion of the supernatant was analyzed by HPLC with a radioactivity detector (Radiomatic 150TR, Packard, Meriden, CT). A YMC-Pack ODS-A column (10 mm inner diameter (i.d.) × 150 mm, YMC, Kyoto, Japan) was used with acetonitrile/50 mM acetic acid/50 mM sodium acetate, pH 4.5 (80/10/10, v/v) at a flow rate of 2 mL/min. The retention times of [^{11}C]CB184 and [^{11}C]CB190 were 10.7 and 9.2 min, respectively. The recovery in the eluate of the injected radioactivity was essentially quantitative.

PET study

Using male Wistar rats (270–370 g), general anesthesia was induced by administering pentobarbital (50 mg/kg). After immobilizing the head using a brain stereotactic apparatus (Narishige, Tokyo, Japan), an incision was placed on the scalp to expose the skull. Using a bone drill, a hole was made in the skull to an area that was 0.4 mm anterior, 3 mm lateral, and 4.5 mm ventral to the bregma (point on the skull where the coronal and sagittal sutures converge), and solution of 6-hydroxydopamine (6-OHDA, 10 μg, Sigma-Aldrich, St. Louis, MO) in 2.5 μL physiological saline was directly injected into the right striatum [26].

Four days after the operation, the rat was anesthetized by 2 % isoflurane in O_2 (2 L/min) and placed in PET gantry of animal PET/CT system (FX-3200, Gamma Medica-Ideas, Northridge, CF) [27]. [^{11}C]CB184 or [^{11}C](*R*)-PK11195 was injected through tail vain and list-mode PET scan was carried out for 60 min. Scans by the radioligands with high and low specific radioactivity were available as we tried serial two scans from one batch of the each tracer. Injected dose is summarized in Table 5. CT data were obtained after the completion of PET acquisition. PET images were reconstructed using 3D maximum likelihood expectation maximization (MLEM) algorithm. Regions of interest (ROIs) were placed on right or left stratum with the aid of superimposed CT scull images using PMOD (PMOD Technologies, Zuerich, Switzerland). Data were expressed in standardized uptake value (SUV).

Time-activity curve (TAC) thus obtained was analyzed by indirect Logan plot method as reported by Converse [28, 29] for [^{11}C](*R*)-PK111195 employing uptake of the lesioned side as target and the contralateral side as reference. The same method was also applied to [^{11}C]CB184 in this study. The slope of the plot derives distribution volume ratio (DVR)—the ratio of distribution volume of right (6-OHDA lesioned) stratum to distribution volume of left stratum. Data were analyzed one-way ANOVA with Bonferroni's correction. Differences were considered significant at a p value less than 0.0083.

Histochemical examination

After euthanasia of the rat used in PET experiment, brain was removed and perfused for histological evaluation according to our report [10]. Numbers of tyrosine hydroxylase (TH) positive neurons were counted. Expression of mRNA coding tumor necrosis factor α (TNF-α) and interleukin-1β (IL-1β) was quantified using a RT-PCR method which was normalized by expression of NADPH [10]. Correlation between histochemistry and PET DVR was examined with Fisher's transformation which derived correlation coefficient (R) and critical value (p).

Table 2 Receptor binding affinity and partition coefficient

K_i (nM)			Log *P*	
Compound	TSPO	CBR	Calculated	Measured
CB148	0.203[a]	6880[a]	5.88[a]	2.20 ± 0.06[a]
CB184	0.537	>10000	4.99	2.06 ± 0.02[b]
CB190	0.882	>10000	3.93	2.39 ± 0.03[b]
(*R*)-PK11195	4.269[a]	7590[a]		2.54 ± 0.05[a]

[a] Data from literature [24]

[b] Mean ± SD of three runs

Results

Binding affinity octanol/water partition coefficient

Binding affinity of CB184, CB190, CB148 and (*R*)-PK11195 toward TSPO and CBR are shown in Table 2. Calculated and measured Log P values were also tabulated. Three CB compounds showed from 4.8 to 21 times higher affinity toward TSPO than (*R*)-PK11195. Selectivity of CB184 and CB190 was also higher than the other two. Especially, binding of CB184 or CB190 to CBR was under detectable range. Measured Log *P* values were similar among CB compounds, however, calculated Log *P* values were different from measured values as we previously reported [24].

Radiochemistry

Radiosynthesis of [^{11}C]CB184 and [^{11}C]CB190 could be achieved with [^{11}C]methyl triflate and acetone as reaction solvent. Decay-corrected radiochemical yield was 73 ± 12 % (n = 8) based on total [^{11}C]methyl triflate used in the synthesis and no difference between two compounds was observed. Time required for synthesis was 34 ± 2 min from the end of irradiation. The specific radioactivity was 184 ± 80 GBq/μmol (n = 8) at the end of synthesis, and the radiochemical purity was over 95 %.

Distribution of [^{11}C]CB184 and [^{11}C]CB190 in organs and brain regions

The organ distribution of radioligands was determined (Table 3) after tail vein injection of [^{11}C]CB184, [^{11}C]CB190 or [^{11}C](*R*)-PK11195. A high initial concentration of radioactivity was found in the lung, heart, and kidney. In Fig. 3, [^{11}C]CB184 and [^{11}C]CB190 showed similar time courses of regional brain distribution as [^{11}C]CB148 in the same experimental system [24]. The cerebellum and olfactory bulb showed more uptake than the other brain regions. [^{11}C](*R*)-PK11195 cleared more rapidly than three CB compounds.

Table 3 Organ distribution of radioactivity after intravenous injection of [^{11}C]CB184 and [^{11}C]CB190 into mice

Organ	Time after injection (min)				
	1	5	15	30	60
[^{11}C]CB184 uptake (%ID/g)					
Blood	5.14 ± 0.33	3.41 ± 0.56	1.51 ± 0.23	0.96 ± 0.26	0.64 ± 0.08
Heart	13.23 ± 1.44	12.34 ± 2.52	13.18 ± 5.51	13.83 ± 2.08	7.72 ± 1.69
Lung	94.82 ± 33.08	54.35 ± 15.27	25.30 ± 14.71	33.19 ± 18.49	13.82 ± 2.33
Liver	2.06 ± 3.31	9.81 ± 4.52	11.15 ± 7.75	2.69 ± 0.94	6.66 ± 1.75
Pancreas	3.66 ± 0.88	4.28 ± 1.40	5.49 ± 0.98	3.00 ± 0.87	3.57 ± 0.82
Spleen	4.12 ± 1.80	19.58 ± 6.59	13.78 ± 0.89	6.51 ± 2.13	10.08 ± 0.50
Kidney	9.04 ± 1.67	13.06 ± 2.68	42.55 ± 32.24	10.99 ± 1.93	11.69 ± 2.56
Intestine	4.47 ± 0.88	6.33 ± 2.91	3.58 ± 1.89	8.07 ± 4.84	5.08 ± 1.87
Testis	0.63 ± 0.41	1.10 ± 0.61	0.70 ± 0.30	0.58 ± 0.17	0.73 ± 0.09
[^{11}C]CB190 uptake (%ID/g)					
Blood	3.73 ± 0.83	2.42 ± 1.20	1.03 ± 0.22	0.70 ± 0.0.13	0.59 ± 0.10
Heart	15.03 ± 2.17	14.45 ± 1.85	11.74 ± 1.78	9.84 ± 1.84	10.55 ± 7.26
Lung	84.23 ± 28.14	42.18 ± 15.34	27.61 ± 6.57	19.39 ± 3.16	51.52 ± 29.19
Liver	2.65 ± 0.58	3.04 ± 0.31	5.46 ± 1.17	5.10 ± 0.77	2.09 ± 1.32
Pancreas	4.08 ± 1.23	4.40 ± 0.57	5.15 ± 0.46	4.78 ± 1.29	3.24 ± 1.74
Spleen	3.95 ± 1.39	7.59 ± 1.85	11.05 ± 2.47	11.64 ± 1.49	4.31 ± 3.12
Kidney	10.60 ± 3.43	12.92 ± 2.46	17.51 ± 0.56	15.04 ± 2.77	8.98 ± 4.94
Intestine	4.43 ± 0.55	5.47 ± 1.10	4.93 ± 1.64	3.87 ± 2.11	3.48 ± 2.59
Testis	0.86 ± 0.55	0.95 ± 0.20	1.06 ± 0.27	0.94 ± 0.15	0.62 ± 0.46

Data represent mean ± SD of four animals

Blocking studies

In vivo selectivity and specificity of [^{11}C]CB184 and [^{11}C]CB190 were examined by pretreatment with PK11195 or flumazenil. Uptake of the each radioligand in brain regions was measured at 30 min post-injection as the uptake levels were observed almost stable from 30 to 60 min post-injection. The uptake of [^{11}C]CB184 was significantly reduced relative to controls in every brain region by PK11195 (Table 4). Flumazenil had little effect on the uptake. In contrast, high uptakes of [^{11}C]CB190 in the cerebellum and olfactory bulb were significantly decreased along with PK11195 treatment, however, the other brain regions did not show the reduction. Similarly, inhibition of [^{11}C](*R*)-PK11195 uptake by cold PK11195 could not be observed in the pons and thalamus.

Metabolite studies

In HPLC analysis of plasma of mice given [^{11}C]CB184, two major radioactive peaks with the retention times of 3.5 and 5.7 min were detected except for [^{11}C]CB184 (retention time of 10.7 min). In the case of [^{11}C]CB190 (retention time 9.2 min), two major radioactive peaks were also found in the retention times of 3.5 and 5.5 min, and several minor metabolites were detected between 2.2 and 3.5 min. In the brain, the radioactive peaks in the retention times of 3.5 min were also found in addition to unchanged form of both tracers. At 30 min after injection of tracer, the percentages of the unchanged form in the brain and plasma were 92.7 ± 5.8 and 36.2 ± 15.5 %, respectively, for [^{11}C]CB184, and the corresponding figures for [^{11}C]CB190 were 86.5 ± 2.8 and 25.6 ± 7.1 %.

Animal PET studies

Time-activity curve after intravenous injection of [^{11}C](*R*)-PK11195 or [^{11}C]CB184 are shown in Fig. 4. Right and left striatum showed similar TACs when radioligands were injected in control animals (Fig. 4a, c). In contrast, 6-OHDA lesion resulted in increased uptake of both radioligands in lesioned side compared to contralateral side (Fig. 4b, d). Visual inspection revealed [^{11}C](*R*)-PK11195 was cleared more rapidly than [^{11}C]CB184. Although we tried serial two PET scans from one batch of the each tracer, the difference of pharmacological dose between low and high dose groups (Table 5) did not affect striatal uptake of both tracers (data are not shown). TACs thus obtained were analyzed by an indirect Logan plot method as reported by Converse for [^{11}C](*R*)-PK11195 employing uptake of the lesioned side as target and the contralateral side as Reference [28, 29]. Figure 5 shows satisfactory linear fitting of [^{11}C](*R*)-PK11195 or [^{11}C]CB184 in both control and lesioned animals. DVRs of [^{11}C](*R*)-PK11195

Table 4 Regional brain distribution of [^{11}C]CB184, [^{11}C]CB190 and [^{11}C](*R*)-PK11195 in mice after treatment with unlabeled drugs

Region	Injected drug		
	Control	PK11195	Flumazenil
[^{11}C]CB184 uptake (%ID/g)			
Olfactory bulb	1.45 ± 0.03	0.92 ± 0.11*	1.36 ± 0.30
Cortex	0.986 ± 0.073	0.594 ± 0.037*	0.965 ± 0.075
Striatum	0.864 ± 0.135	0.616 ± 0.026	0.806 ± 0.141
Hippocampus	1.225 ± 0.067	0.659 ± 0.099*	1.087 ± 0.122
Thalamus	0.985 ± 0.042	0.625 ± 0.024*	0.908 ± 0.159
Midbrain	0.965 ± 0.071	0.626 ± 0.031*	0.994 ± 0.228
Cerebellum	1.384 ± 0.091	0.729 ± 0.057*	1.361 ± 0.185
Pons	1.045 ± 0.102	0.655 ± 0.045*	1.003 ± 0.180
[^{11}C]CB190 uptake (%ID/g)			
Olfactory bulb	1.434 ± 0.090	1.026 ± 0.277*	1.329 ± 0.183
Cortex	0.838 ± 0.072	0.731 ± 0.227	0.722 ± 0.080
Striatum	0.715 ± 0.052	0.738 ± 0.235	0.704 ± 0.115
Hippocampus	0.887 ± 0.171	0.763 ± 0.134	0.643 ± 0.083
Thalamus	0.761 ± 0.084	0.702 ± 0.220	0.718 ± 0.097
Midbrain	0.950 ± 0.062	0.781 ± 0.214	0.830 ± 0.313
Cerebellum	1.363 ± 0.046	0.849 ± 0.232*	1.223 ± 0.275
Pons	0.890 ± 0.076	0.682 ± 0.199	0.793 ± 0.122
[^{11}C](*R*)-PK11195 uptake (%ID/g)			
Olfactory bulb	1.129 ± 0.107	0.481 ± 0.240*	1.015 ± 0.218
Cortex	0.626 ± 0.191	0.409 ± 0.112	0.606 ± 0.048
Striatum	0.507 ± 0.090	0.308 ± 0.089	0.634 ± 0.205
Hippocampus	0.730 ± 0.225	0.390 ± 0.054	0.746 ± 0.248
Thalamus	0.578 ± 0.297	0.431 ± 0.205	0.456 ± 0.068
Midbrain	0.610 ± 0.056	0.359 ± 0.052*	0.648 ± 0.134
Cerebellum	1.230 ± 0.243	0.389 ± 0.025*	1.171 ± 0.222
Pons	1.129 ± 0.107	0.481 ± 0.240	1.015 ± 0.218

Data represent mean ± SD of four animals. Blocking drugs were intravenously injected 1 min prior to the tracer administration. Data were analyzed 1-way ANOVA with Bonferroni's correction. Differences were considered significant at a p value less than 0.0167 (*)

in control and lesioned animals were 1.02 ± 0.08 ($n = 4$) and 1.15 ± 0.10 ($n = 5$), respectively, (mean ± SD). DVRs for [^{11}C]CB184 in control and lesioned animals were 1.03 ± 0.03 ($n = 4$) and 1.15 ± 0.09 ($n = 6$), respectively. Both radioligands showed significantly different DVR values between control and lesioned rats.

Correlations between the DVR values for [^{11}C](*R*)-PK11195 or [^{11}C]CB184 and histochemical data were examined. Data for both control and 6-OHDA treated rats are plotted in Fig. 6. Significant correlation ($p < 0.05$) was only seen between [^{11}C](*R*)-PK11195 and TH (Fig. 6a). Correlation between [^{11}C]CB184 and TH (Fig. 6d, $p = 0.06$) was not statistically significant, however, this would be expected with increasing number of data. The tendencies of positive correlation between DVR of [^{11}C](*R*)-PK11195 or [^{11}C]CB184 and expression of TNFα or IL-1β expression were also observed in spite they lack statistical significance (Fig. 6b, c, e, f).

Discussion

We previously reported preparation and biodistribution of four TSPO radioligands with imidazopyridineacetamide structure [24] via *N*-[^{11}C]methylation reaction. Among those, only [^{11}C]CB148 (compound **[^{11}C]7** in the previous paper) showed positive results. We are presenting herewith two another compounds of this class, [^{11}C]CB184 and [^{11}C]CB190. Radiosynthesis of these novel compounds is quite straightforward. Using [^{11}C]methyl triflate, these compounds were obtained with radiochemical yield of 73 % (decay-corrected). *O*-[^{11}C]Methylation of the phenolic hydroxyl group in the presence of small amount of NaOH should be regarded as the first choice in labeling strategy.

In vivo validation as a TSPO radioligand was firstly carried out following our previous report using normal mice [24]. In addition, an animal PET study using 6-OHDA treated rats as a model of neurodegeneration was pursued for proper estimation of feasibility of the radioligands to determine neuroinflammation process. In mice, among the brain regions examined, cerebellum and olfactory bulb showed the highest uptake of the every tracer examined. Even in normal rodents, microglia cells are present in all major divisions of brain [30]. Higher density of TSPO in the olfactory bulb of normal rodents is consistent across publications, however, TSPO density in the cerebellum should be different between animal species. In the normal rat brain cerebellar TSPO is reported to be negligible or one of the lowest among brain regions. In contrast, experiments employing mice are consistently reporting higher uptake of TSPO radioligands in cerebellum together with olfactory bulb [16, 17, 31]. In the present article [^{11}C]CB184 showed almost same performance as our previous compound [^{11}C]CB148 from regional brain distribution (Fig. 3) and from the blocking experiment (Table 3). Suppressed uptake of [^{11}C]CB190 along with pretreatment with cold PK11195 was found in limited areas in spite these two compounds share the similar TSPO binding affinity and partition coefficient. It is noteworthy that partition coefficients obtained by shaking-flask method and by CLOGP program calculation showed great difference. This situation is in accordance with our previous report [24]. At present we can not define the reason for this, however, the importance of direct measurement of partition coefficient was highlighted, again.

A rat-PET study in an injured brain model enabled more adequate expectation of feasibility of the radioligand in

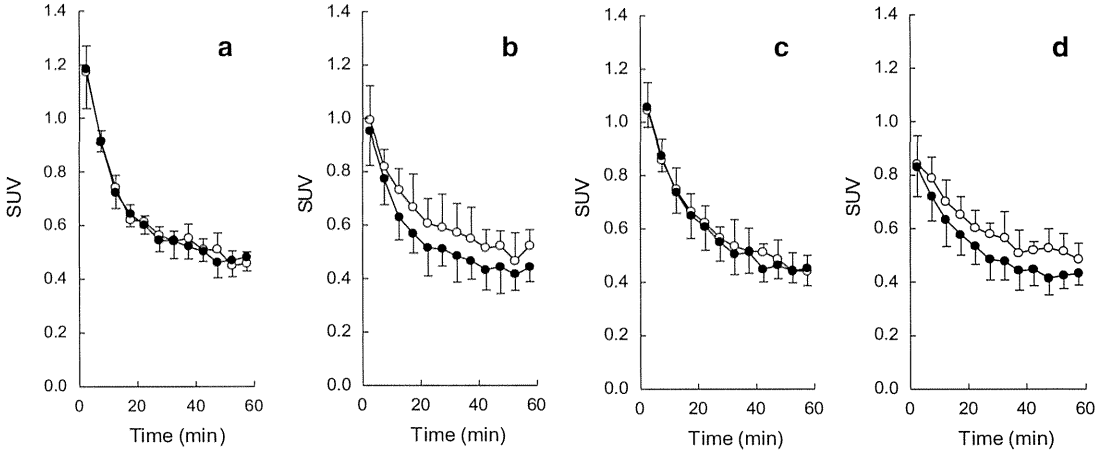

Fig. 4 Time-activity curves after i.v. injection of [^{11}C](*R*)-PK11195 or [^{11}C]CB184 to 6-OHDA lesioned rats; standardized uptake value (SUV) after intravenous injection of [^{11}C](*R*)-PK11195 (**a**, **b**) or [^{11}C]CB184 (**c**, **d**) into control (**a**, **c**) or 6-OHDA injured rat (**b**, **d**) are shown. *Open circle* shows *right* (injured) striatum and *closed circle* shows contralateral (*left*) striatum. Data are expressed as SUV (mean and SD of four animals)

Table 5 Doses of radioligands used in animal PET studies

	Radioactivity (MBq)	Pharmacological dose (nmol)		
		Total (*n*)	Low dose group (*n*)	High dose group (*n*)
[^{11}C](*R*)-PK11195	28.9 ± 6.6	2.41 ± 4.11 (9)	0.36 ± 0.28 (4)	4.45 ± 5.25 (5)
[^{11}C]CB184	29.1 ± 5.6	1.39 ± 1.96 (10)	0.19 ± 0.11 (5)	2.60 ± 2.23 (5)

Radioactivity and pharmacological dose of [^{11}C](*R*)-PK11195 and [^{11}C]CB184 were indicated. Data represent mean and SD. Number of animals was shown in the parenthesis

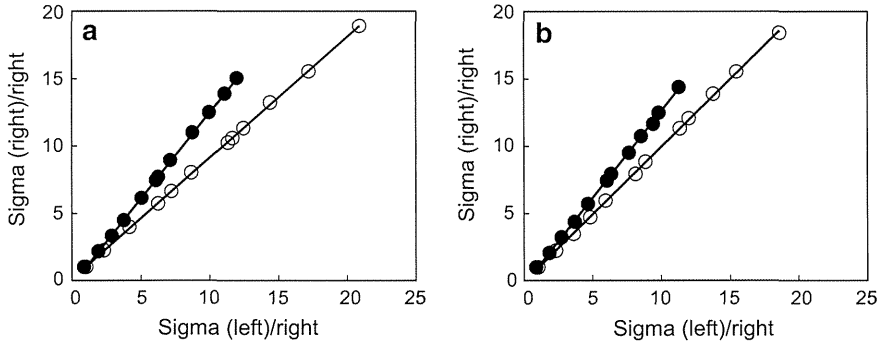

Fig. 5 Logan plot analysis; representative indirect Logan plot analysis [28, 29] of *right* and *left* striatal uptake of control (*open circle*) or 6-OHDA injured (*closed circle*) rat after intravenous injection of [^{11}C](*R*)-PK11195 (**a**) or [^{11}C]CB184 (**b**) in a rat. The analyses were carried out employing uptake of the lesioned side as target and the contralateral side as reference. After linear regression of the each plot, distribution volume ratio (DVR) between *right* and *left* striatum was obtained from its slope (see text)

patients with neurodegenerative disease. Figure 4 clearly shows that the 6-OHDA injured striatum has more uptake of TSPO tracers compared to contralateral side. Visual inspection of Fig. 4 reveals that [^{11}C]CB184 has slower washout from the rat brain than [^{11}C](R)-PK11195 due to higher binding affinity of the compound in either control or injured tissue. This tendency was in accordance with the result of mouse experiment (Fig. 3).

As TSPO is thought to exist even in normal brain tissue, the contrast between lesioned and normal brain tissue as shown in Fig. 4 does not indicate specific binding of the tracer to TSPO. It might only indicate the lesion-related

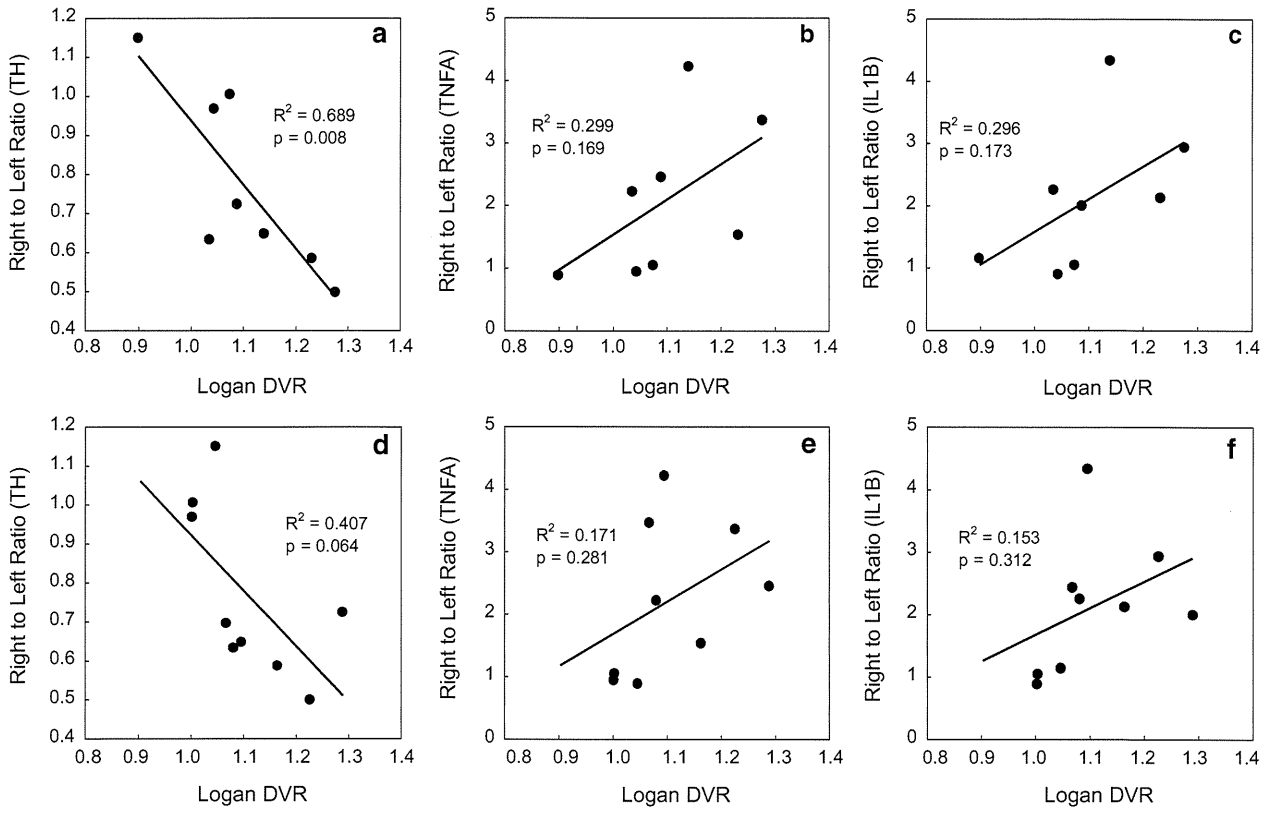

Fig. 6 Correlation between Logan DVR and *right* to *left* ratio of histochemical measures; correlation between Logan DVR and *right* to *left* ratio of number of tyrosine hydroxylase (TH) positive cell (**a**, **d**), of mRNA expression of tumor necrosis factor α (TNFA) (**b**, **e**) or interleukin-1β (IL1B) (**c**, **f**) after intravenous injection of [^{11}C](*R*)-PK11195 (**a**–**c**) or [^{11}C]CB184 (**d**–**f**) was examined. Both data from control and 6-OHDA reated rats were plotted. mRNA expression level (TNFα and IL-1β) was normalized by expression of NADPH. Data were analyzed for their correlation with Fisher's transformation. (n = 9 and 10 for [^{11}C]CB184 and [^{11}C](*R*)-PK11195, respectively). Regression coefficient (R^2) and critical value (p) are shown

elevation of inflammatory activity. Converse et al. [28] reported an indirect Logan plot analysis for [^{11}C](*R*)-PK11195 employing contralateral brain tissue as a reference region [29]. We also attempted this analysis and fair plot fitting and adequate DVR was obtained for both [^{11}C]CB184 and [^{11}C](*R*)-PK11195 (Fig. 5). 6-OHDA treated animals showed significantly higher DVR than non-lesioned animals for both [^{11}C]CB184 and [^{11}C](*R*)-PK11195 and the DVR shows the lesion-related elevation of inflammatory activity. DVR in 6-OHDA treated rat was 1.15 ± 0.10 for [^{11}C](*R*)-PK11195 and was 1.15 ± 0.09 for [^{11}C]CB184. These values showed no difference from ANOVA analysis and, therefore, sensitivity to detect neuroinflammation activity was similar for these two compounds.

Although we tried serial two PET scans from one batch of the each tracer, the two different pharmacological doses shown in Table 5 did not affect striatal uptake of both tracers (data not shown). As those high doses ranged from 1.3 to 6.6 nmol (from 1.6 to 7.8 μg/kg) high-end values should be regarded as maximum dose limit ensuring reproducible measurement due to low receptor occupancy. Boutin also reported that 23.7 nmol of [^{11}C](*R*)-PK11195 did not affect significantly the TACs or the contrast between the ipsilateral and contralateral side or the binding potential values [32]. Our result is in good accordance with this report.

In vivo metabolism studies showed that 36 and 25 % of radioactivity in plasma remained unchanged 30 min after intravenous injection of [^{11}C]CB184 and [^{11}C]CB190, respectively, (Table 6). It is clear contrast to the observation of [^{11}C]CB148 on which 83 % of radioactivity was observed unchanged by the same experimental system [24]. This could be explained from the difference in labeling position. As these three compounds share the *N*-dialkylacetamide substructure, a rather stable feature of [^{11}C]CB148 will explain resistance of this structure toward metabolism, however, a small amount (5 %) of polar

Table 6 Metabolite analysis

	[^{11}C]CB184		[^{11}C]CB190	
	Extraction yield (%)	Unchanged form (%)	Extraction yield (%)	Unchanged form (%)
Plasma	80.3 ± 3.3	36.2 ± 15.5	96.6 ± 3.3	25.6 ± 7.1
Brain	99.6 ± 0.1	92.7 ± 5.8	99.7 ± 0.3	86.5 ± 2.8

Data represent means and SD of three animals

metabolite was found in the brain [24]. On the other hand, polar metabolite in brain tissue was negligible for either [^{11}C]CB184 or [^{11}C]CB190.

Finally, we examined the relationship between DVR of [^{11}C](*R*)-PK11195 or [^{11}C]CB184 and histochemistry measures. We counted TH positive cells and quantified expression of inflammatory cytokines, TNFα and IL-1β mRNA by RT-PCR (Fig. 6) following our previous report [10]. We only could detect significant relationship between [^{11}C](*R*)-PK11195 DVR and left-to-right ratio of number of TH positive cells. Almost the same results were obtained when we employed right-to-left ratio of SUV value from 30 to 60 min after injection of an either radioligand (data not shown). Tight relationship between the histochemistry measures and the uptake of TSPO ligand could not be exhibited in the present examination because of limited statistical power. However, the direct comparison of PET results and inflammation indexes which can only be obtained by animal experiment will provide information concerning mechanisms underlying neurodegeneration and TSPO activation.

Recently, Yasuno et al. [33] reported that phonoxyphenyl acetamide, [^{11}C]DAA1106 binding to TSPO was significantly increased in widespread areas in subjects with mild cognitive impairment which is a prodromal state of Alzheimer's disease and this increased binding could be utilized to predict development of dementia. But a recent clinical PET study using [^{11}C]PBR28 has reported that 14 % of healthy volunteers did not have a specific binding signal in either the brain or the peripheral organs [34]. This individual difference of binding was not observed for [^{11}C](*R*)-PK11195 [35] and the similar controversy should be expected for structurally related [^{11}C]PBR06, [^{18}F]FEPPA as well as DAA family compounds. So another candidate of TSPO ligand with different structural class should be desirable also from this viewpoint.

In conclusion, we report synthesis of two carbon-11 labeled imidazopyridines TSPO ligands, [^{11}C]CB184 and [^{11}C]CB190, for PET imaging of neuroinflammation. These compounds were readily prepared by *O*-methylation reaction using [^{11}C]methyl triflate. In mice, [^{11}C]CB184 showed more uptake and specific binding than [^{11}C]CB190. In PET study using 6-OHDA treated rats, lesioned side of the brain showed higher uptake than contralateral side after i.v. injection of either [^{11}C]CB184 or [^{11}C](*R*)-PK11195. Indirect Logan plot analysis revealed distribution volume ratio (DVR) between the two sides which might indicate lesion-related elevation of TSPO binding. DVR in 6-OHDA treated mouse was 1.15 ± 0.10 for [^{11}C](*R*)-PK11195 and was 1.15 ± 0.09 for [^{11}C]CB184. These values indicate that the sensitivity to detect neuroinflammation activity was similar for these two compounds.

Acknowledgments The authors would like to thank the members of National Center for Geriatrics and Gerontology for their help. This work was supported by the Research Funding for Longevity Sciences from National Center for Geriatrics and Gerontology, Japan (21-5). All the authors disclose to have no potential conflict of interest.

References

1. Papadopoulos V, Baraldi M, Guilarte TR, Knudsen TB, Lacapère JJ, Lindemann P, et al. Translocator protein (18 kDa): new nomenclature for the peripheral-type benzodiazepine receptor based on its structure and molecular function. Trends Pharmacol Sci. 2006;27:402–9.
2. Culty M, Li H, Boujrad N, Amri H, Vidic B, Bernassau JM, et al. In vitro studies on the role of the peripheral-type benzodiazepine receptor in steroidogenesis. J Steroid Biochem Mol Biol. 1999;69:123–30.
3. Szabo I, De Pinto V, Zoratti M. The mitochondrial permeability transition pore may comprise VDAC molecules. II. The electrophysiological properties of VDAC are compatible with those of the mitochondrial megachannel. FEBS Lett. 1993;330:206–10.
4. Golani I, Weizman A, Leschiner S, Spanier I, Eckstein N, Limor R, et al. Hormonal regulation of peripheral benzodiazepine receptor binding properties is mediated by subunit interaction. Biochemistry. 2001;40:10213–22.
5. Beurdeley-Thomas A, Miccoli L, Oudard S, Dutrillaux B, Poupon MF. The peripheral benzodiazepine receptors: a review. J Neuro Oncol. 2000;46:45–56.
6. Lacapere JJ, Papadopoulos V. Peripheral-type benzodiazepine receptor: structure and function of a cholesterol-binding protein in steroid and bile acid biosynthesis. Steroids. 2003;68:569–85.
7. Banati RB. Visualizing microglia activation in vivo. Glia. 2002;40:206–17.
8. Venneti S, Lopresti B, Wiley CA. The peripheral benzodiazepine receptor in microglia: from pathology to imaging. Prog Neurobiol. 2006;80:308–22.
9. Kreutzberg GW. Microglia; a sensor for pathological events in the CNS. Trends Neurosci. 1996;19:312–8.
10. Ito F, Toyama H, Kudo G, Suzuki H, Hatano K, Ichise M, et al. Two activated stages of microglia and PET imaging of peripheral benzodiazepine receptors with [^{11}C]PK11195 in rats. Ann Nucl Med. 2010;24:163–9.
11. Shah F, Hume S, Pike V, Ashworth S, McDermott J. Synthesis of the enantiomers of [*N*-methyl-^{11}C]PK 11195 and comparison of

their behaviors as radioligands for PK binding sites in rats. Nucl Med Biol. 1994;21:573–81.
12. Belloli S, Moresco RM, Matarrese M, Biella G, Sanvito F, Simonelli P, et al. Evaluation of three quinoline carboxamide derivatives as potential radioligands for the in vivo PET imaging of neurodegeneration. Neurochem Int. 2004;44:433–40.
13. Petit-Taboué MC, Baron JC, Barré L, Travère JM, Speckel D, Camsonne R, et al. Brain kinetics and specific binding of [^{11}C]PK 11195 to omega 3 sites in baboons: positron emission tomography study. Eur J Pharmacol. 1991;200:347–51.
14. Kropholler MA, Boellaard R, Schuitemaker A, van Berckel BN, Luurtsema G, Windhorst AD, et al. Development of a tracer kinetic plasma input model for (*R*)-[11C]PK11195 brain studies. J Cereb Blood Flow Metab. 2005;25:842–51.
15. Lockhart A, Davis B, Matthews JC, Rahmoune H, Hong G, Gee A, et al. The peripheral benzodiazepine receptor ligand PK11195 binds with high affinity to the acute phase reactant alpha1-acid glycoprotein: implications for the use of the ligand as a CNS inflammatory marker. Nucl Med Biol. 2003;30:199–206.
16. Zhang M-R, Kida T, Noguchi J, Furutsuka K, Maeda J, Suhara T, et al. [^{11}C]DAA1106: radiosynthesis and in vivo binding to peripheral benzodiazepine receptors in mouse brain. Nucl Med Biol. 2003;30:513–9.
17. Zhang MR, Maeda J, Ogawa M, Noguchi J, Ito T, Yoshida Y, et al. Development of a new radioligand, *N*-(5-fluoro-2-phenoxyphenyl)-*N*-(2-[^{18}F]fluoroethoxyl-5-methoxy benzyl)acetamide, for PET imaging of peripheral benzodiazepine receptor in primate brain. J Med Chem. 2004;47:2228–35.
18. Briard E, Zoghbi S, Imaizumi M, Gourley J, Shetty U, Hong J, et al. Synthesis and evaluation of two sensitive ^{11}C-labeled aryloxyanilide ligands for imaging brain peripheral benzodiazepine receptors in vivo. J Med Chem. 2008;51:17–30.
19. Wilson A, Garcia A, Parkes H, McCormick P, Stephenson K, Houle S, et al. Radiosynthesis and initial evaluation of [^{18}F]-FEPPA for PET imaging of peripheral benzodiazipine receptors. Nucl Med Biol. 2008;35:305–14.
20. James M, Fulton R, Henderson D, Eberl S, Meikle S, Thomson S, et al. Synthesis and in vivo evaluation of a novel peripheral benzodiazepine receptor PET radioligand. Bioorg Med Chem. 2005;13:6188–94.
21. Martín A, Boisgard R, Thézé B, Van Camp N, Kuhnast B, Damont A, et al. Evaluation of the PBR/TSPO radioligand [(18)F]DPA-714 in a rat model of focal cerebral ischemia. J Cereb Blood Flow Metab. 2010;30:230–41.
22. Zhang M, Kumata K, Maeda J, Yanamoto K, Hatori A, Okada M, et al. ^{11}C-AC-5216: a novel PET ligand for peripheral benzodiazepine receptors in the primate brain. J Nucl Med. 2007;48:1853–61.
23. Mattner F, Mardon K, Katsfis A. Pharmacological evaluation of [^{123}I]-CLINDE: a radioiodinated imidazopyridine-3-acetamide for the study of peripheral benzodiazepine binding sites (PBBS). Eur J Nucl Med Mol Imaging. 2008;35:779–89.
24. Sekimata K, Hatano K, Ogawa M, Abe J, Magata Y, Biggio G, et al. Radiosynthesis and in vivo evaluation of *N*-[^{11}C]methylated imidazopyridineacetamides as PET tracers for peripheral benzodiazepine receptors. Nucl Med Biol. 2008;35:327–34.
25. Denora N, Laquintana V, Pisu MG, Dore R, Murru L, Latrofa A, Trapani G, Sanna E. 2-Phenyl-imidazo[1,2-a]pyridine compounds containing hydrophilic groups as potent and selective ligands for peripheral benzodiazepine receptors: synthesis, binding affinity and electrophysiological studies. J Med Chem. 2008;2008(51):6876–87.
26. Toyama H, Hatano K, Suzuki H, Ichise M, Momosaki S, Kudo G, et al. In vivo imaging of microglial activation using a peripheral benzodiazepine receptor ligand: [^{11}C]PK-11195 and animal PET following ethanol injury in rat striatum. Ann Nucl Med. 2008;22:417–24.
27. Bergeron M, Cadorette J, Beaudoin JF, Lepage MD, Robert G, Selivanov V, et al. Performance evaluation of the LabPET APD-based digital PET scanner. IEEE Trans Nulc Sci. 2009;56:10–6.
28. Converse AK, Larsen EC, Engle JW, Barnhart TE, Nickles RJ, Duncan ID. ^{11}C-(R)-PK11195 PET imaging of microglial activation and response to minocycline in Zymosan-treated rats. J Nucl Med. 2011;52:257–62.
29. Logan J, Fowler JS, Volkow ND, Wang GJ, Ding YS, Alexoff DL. Distribution volume ratios without blood sampling from graphical analysis of PET data. J Cereb Blood Flow Metab. 1996;16:834–40.
30. Lawson LJ, Perry VH, Dri P, Gordon S. Heterogeneity in the distribution and morphology of microglia in the normal adult mouse brain. Neurosci. 1990;39:151–70.
31. Chen MK, Baidoo K, Verina T, Guilarte TR. Peripheral benzodiazepine receptor imaging in CNS demyelination: functional implications of anatomical and cellular localization. Brain. 2004;127:1379–92.
32. Boutin H, Chauveau F, Thominiaux C, Gregoire MC, James ML, Trebossen R, Hantraye P, Dolle F, Tavitian B, Kassiou M. ^{11}C-DPA-713: a novel peripheral benzodiazepine receptor PET ligand for in vivo imaging of neuroinflammation. J Nucl Med. 2007;48:573–81.
33. Yasuno F, Kosaka J, Ota M, Higuchi M, Ito H, Fujimura Y, Nozaki S, Takahashi S, Mizukami K, Asada T, Suhara T. Increased binding of peripheral benzodiazepine receptor in mild cognitive impairment-dementia converters measured by positron emission tomography with [(11)C]DAA1106. Psychiatry Res. 2012;203:67–74.
34. Fujita M, Imaizumi M, Zoghbi SS, Fujimura Y, Farris AG, Suhara T, Hong J, Pike VW, Innis RB. Kinetic analysis in healthy humans of a novel positron emission tomography radioligand to image the peripheral benzodiazepine receptor, a potential biomarker for inflammation. Neuroimage. 2008;40:43–52.
35. Owen DR, Howell OW, Tang SP, Wells LA, Bennacef I, Bergstrom M, Gunn RN, Rabiner EA, Wilkins MR, Reynolds R, Matthews PM, Parker CA. Two binding sites for [^{3}H]PBR28 in human brain: implications for TSPO PET imaging of neuroinflammation. J Cereb Blood Flow Metab. 2010;30(9):1608–18.

Journal of Alzheimer's Disease xx (20xx) x–xx
DOI 10.3233/JAD-141338
IOS Press

Prediction of Outcomes in Mild Cognitive Impairment by Using ^{18}F-FDG-PET: A Multicenter Study

Kengo Ito[a,b,*], Hidenao Fukuyama[c], Michio Senda[d], Kazunari Ishii[e], Kiyoshi Maeda[f], Yasuji Yamamoto[g], Yasuomi Ouchi[h], Kenji Ishii[i], Ayumu Okumura[j], Ken Fujiwara[a], Takashi Kato[a], Yutaka Arahata[k], Yukihiko Washimi[k], Yoshio Mitsuyama[l], Kenichi Meguro[m], Mitsuru Ikeda[n] and SEAD-J Study Group

[a]*Department of Clinical and Experimental Neuroimaging, National Center for Geriatrics and Gerontology, Obu-shi, Aichi, Japan*
[b]*Department of Radiology, National Center for Geriatrics and Gerontology, Obu-shi, Aichi, Japan*
[c]*Human Brain Research Center, Kyoto University, Kyoto, Japan*
[d]*Division of Molecular Imaging, Institute of Biomedical Research and Innovation, Kobe, Japan*
[e]*Department of Radiology, Kinki University, Osaka, University*
[f]*Department of Medical Rehabilitation, Kobe Gakuin University, Kobe, Japan*
[g]*Department of Psychiatry, Kobe University Graduate School of Medicine, Kobe, Japan*
[h]*Medical Photonics Research Center, Hamamatsu University School of Medicine, Hamamatsu, Japan*
[i]*Positron Medical Center, Tokyo Metropolitan Institute of Gerontology, Tokyo, Japan*
[j]*Chubu Medical Center for Prolonged Traumatic Brain Dysfunction, Kizawa Memorial Hospital, Gifu, Japan*
[k]*National Hospital for Geriatric Medicine, National Center for Geriatrics and Gerontology, Obu-shi, Aichi, Japan*
[l]*Psychogeriatric Center, Daigo Hospital, Miyazaki, Japan*
[m]*Department of Geriatric Behavioral Neurology, Tohoku University Graduate School of Medicine, Miyagi, Japan*
[n]*Department of Radiological Technology, Nagoya University School of Health Sciences, Nagoya, Japan*

Handling Associate Editor: Henryk Barthel

Accepted 12 December 2014

Abstract.
Background: ^{18}F-FDG-PET is defined as a biomarker of neuronal injury according to the revised National Institute on Aging–Alzheimer's Association criteria.
Objective: The objective of this multicenter prospective cohort study was to examine the value of ^{18}F-FDG-PET in predicting the development of Alzheimer's disease (AD) in patients with mild cognitive impairment (MCI).
Methods: In total, 114 patients with MCI at 9 participating institutions underwent clinical and neuropsychological examinations, MRI, and ^{18}F-FDG-PET at baseline. The cases were visually classified into predefined dementia patterns by three experts. An automated analysis for ^{18}F-FDG-PET was also performed to calculate the PET score. Subjects were followed periodically for 3 years, and progression to dementia was evaluated.

*Correspondence to: Kengo Ito, Clinical and Experimental Neuroimaging, National Center for Geriatrics and Gerontology, 7-430, Morioka-cho, Obu-shi, Aichi 474-8511, Japan. Tel.: +81 562 46 2311; Fax: +81 562 44 6596; E-mail: kito@ncgg.go.jp.

ISSN 1387-2877/15/$27.50

Results: In 47% of the patients with MCI, progression of symptoms justified the clinical diagnosis of "probable AD". The PET visual interpretation predicted conversion to AD during 3-year follow-up with an overall diagnostic accuracy of 68%. Overall diagnostic accuracy of the PET score was better than that of PET visual interpretation at all follow-up intervals, and the optimized PET score threshold revealed the best performance at the 2-year follow-up interval with an overall diagnostic accuracy of 83%, a sensitivity of 70%, and a specificity of 90%. Multivariate logistic regression analysis identified the PET score as the most significant predictive factor distinguishing AD converters from non-converters.

Conclusion: The PET score is the most statistically significant predictive factor for conversion from MCI to AD, and the diagnostic performance of the PET score is more promising for rapid converters over 2 years.

Keywords: Alzheimer's disease, cerebral glucose metabolism, ^{18}F-FDG-PET, mild cognitive impairment, prospective study

INTRODUCTION

Although an effective treatment for Alzheimer's disease (AD) has not been established, it is possible to delay the progression of symptoms with pharmacological and non-pharmacological treatments. Since pathological changes, such as senile plaques, arise more than 20 years before the manifestation of AD symptomatology, early diagnosis is required for early intervention.

Mild cognitive impairment (MCI) is a diagnostic entity used to describe abnormalities of memory function that do not fulfill the criteria for dementia [1]. MCI includes prodromal AD and other causes of dementia, as well as a form of cognitive impairment that does not progress to dementia and can disappear. Recent progress in basic research on AD and advances in *in vivo* biomarkers have led to a substantial revision of the diagnostic criteria for AD [2] to capture the full spectrum of the disease and to detect its earliest stages [3]. The revised National Institute on Aging–Alzheimer's Association criteria [4–6] suggest that accuracy in diagnosing AD can be improved with information provided by structural and biological evidence of AD pathology. Such information, if discernible at the MCI stage, may allow for differentiation of early AD from MCI owing to other causes [6].

^{18}F-FDG-PET is defined as a biomarker of neuronal injury according to the revised criteria. Studies with ^{18}F-FDG-PET have reported better diagnostic performance than other modalities in distinguishing AD-converters from non-converters in amnestic MCI patients [7–14]. Most studies have shown that the presence of AD-like hypometabolism in the posterior associative and/or posterior cingulate cortex of patients with MCI is predictive of conversion to AD within 1–3 years. However, with the exception of a few studies [11–14], the studies were conducted in relatively small groups of subjects, and follow-up times were not uniform. In this study, we report data from clinical and ^{18}F-FDG-PET assessments within a multicenter prospective cohort study of subjects with amnestic MCI (Study on Diagnosis of Early Alzheimer's Disease-Japan: SEAD-Japan). The objective of this study was to investigate the diagnostic value of ^{18}F-FDG-PET findings suggesting AD-like hypometabolism in predicting MCI conversion to AD, based on a multicenter prospective study.

METHODS

Participating subjects

Subjects with amnestic MCI were recruited between January 2006 and March 2007 and followed up annually for 3 years. Subjects were recruited from memory clinics of 9 centers specializing in AD and other dementias across Japan (Supplementary Table 1). All subjects were living independently in the community at the time of their baseline evaluation. This study was approved by the Ethics Committee at every participating institution. Each subject signed an informed consent form after the nature of the procedures had been fully explained.

All patients were free of significant underlying medical, neurological, or psychiatric illnesses. Patients were initially assessed using a neuropsychological test battery, including the Mini-Mental State Examination (MMSE), Alzheimer's Disease Assessment Scale-cognitive component-Japanese version (ADAS-J cog), Clinical Dementia Rating (CDR), Geriatric Depression Scale (GDS), Everyday Memory Check List (EMCL), and Logical Memory Subset of the Wechsler Memory Scale Revised (WMS-R LM). In accordance with the inclusion criteria, MCI patients were aged between 50 and 80 years, with an MMSE score $\geq$24, a GDS score $\leq$10, a WMS-R LM I score $\leq$13, a LM II part A and part B score (maximum = 50) $\leq$8, and a CDR memory box score equal to 0.5. Patients with formal education for less than 6 years were excluded.